

AD-A249 625



WL-TR-91-2099

Volume 1

DTIC
S **ELECTE** **D**
MAY 7 1992
C



**ADVANCED THERMALLY STABLE, JET FUELS DEVELOPMENT
PROGRAM ANNUAL REPORT**

VOLUME 1 - MODEL AND EXPERIMENT SYSTEM DEVELOPMENT

Elmer Klavetter
Wayne Trott
Tim O'Hern
Steve Martin

Sandia National Laboratories
Albuquerque, NM 87185

January 1992

INTERIM REPORT FOR THE PERIOD JUNE 1990 - JUNE 1991

APPROVED FOR PUBLIC RELEASE; DISTRIBUTION IS UNLIMITED

AERO PROPULSION AND POWER DIRECTORATE
WRIGHT LABORATORY
AIR FORCE SYSTEMS COMMAND
WRIGHT-PATTERSON AFB OH 45433-6563

92-11998



82 5 01 36

NOTICE

When Government drawings, specifications, or other data are used for any purpose other than in connection with a definitely Government-related procurement, the United States Government incurs no responsibility or any obligation whatsoever. The fact that the Government may have formulated or in any way supplied the said drawings, specifications, or other data, is not to be regarded by implication, or otherwise in any manner construed, as licensing the holder, or any other person or corporation; or as conveying any rights or permission to manufacture, use, or sell any patented invention that may in any way be related thereto.

This report is releasable to the National Technical Information Service (NTIS). At NTIS, it will be available to the general public, including foreign nations.

This technical report has been reviewed and is approved for publication.

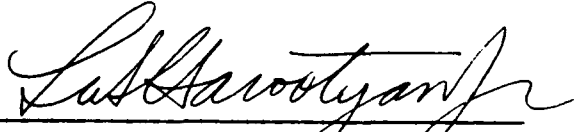


WILLIAM E. HARRISON III
Project Engineer
Fuels Branch



CHARLES L. DELANEY, Chief
Fuels Branch
Fuels and Lubrication Division

FOR THE COMMANDER



LEO S. HAROOTYAN, JR., Chief
Fuels and Lubrication Division
Aero Propulsion and Power Directorate

If your address has changed, if you wish to be removed from our mailing list, or if the addressee is no longer employed by your organization, please notify WL/POSF, WPAFB OH 45433-6563 to help us maintain a current mailing list.

Copies of this report should not be returned unless return is required by security considerations, contractual obligations, or notice on a specific document.

UNCLASSIFIED

SECURITY CLASSIFICATION OF THIS PAGE

REPORT DOCUMENTATION PAGE				Form Approved OMB No. 0704-0188	
1a. REPORT SECURITY CLASSIFICATION Unclassified		1b. RESTRICTIVE MARKINGS None			
2a. SECURITY CLASSIFICATION AUTHORITY N/A		3. DISTRIBUTION / AVAILABILITY OF REPORT Approved for public release; Distribution is unlimited			
2b. DECLASSIFICATION / DOWNGRADING SCHEDULE N/A					
4. PERFORMING ORGANIZATION REPORT NUMBER(S) N/A		5. MONITORING ORGANIZATION REPORT NUMBER(S) WL-TR-91-2099			
6a. NAME OF PERFORMING ORGANIZATION Sandia National Laboratories		6b. OFFICE SYMBOL (if applicable)	7a. NAME OF MONITORING ORGANIZATION Aero Propulsion and Power Lab Air Force Systems Command		
6c. ADDRESS (City, State, and ZIP Code) Albuquerque, NM 87185		7b. ADDRESS (City, State, and ZIP Code) Wright Laboratory WL/POSF Wright-Patterson Air Force Base, OH 45433-6563			
8a. NAME OF FUNDING / SPONSORING ORGANIZATION N/A		8b. OFFICE SYMBOL (if applicable) N/A	9. PROCUREMENT INSTRUMENT IDENTIFICATION NUMBER FY1455-89-NO635		
8c. ADDRESS (City, State, and ZIP Code) N/A		10. SOURCE OF FUNDING NUMBERS			
		PROGRAM ELEMENT NO. 62203F	PROJECT NO. 3048	TASK NO. 05	WORK UNIT ACCESSION NO. 87
11. TITLE (Include Security Classification) Advanced Thermally Stable Jet Fuels Development Program Annual Report Vol 1 - Model and Experiment System Development					
12. PERSONAL AUTHOR(S) E. Klavetter, W. Trott, T. O'Hern and S. Martin					
13a. TYPE OF REPORT Interim		13b. TIME COVERED FROM 6/90 TO 6/91		14. DATE OF REPORT (Year, Month, Day) January 1992	15. PAGE COUNT 58
16. SUPPLEMENTARY NOTATION					
17. COSATI CODES			18. SUBJECT TERMS (Continue on reverse if necessary and identify by block number) Jet Fuels, Thermal Stability, Fouling, Thermal Degradation, Instrumentation, High Temperature Fuels, Laser Diagnostics		
FIELD	GROUP	SUB-GROUP			
19. ABSTRACT (Continue on reverse if necessary and identify by block number) A program entitled "Thermally Stable Jet Fuels Development" was initiated in FY89 by the U.S. Air Force, Aero Propulsion and Power Directorate, working jointly with the Department of Energy, Pittsburgh Energy Technology Center. Aviation turbine fuel thermal stability is of concern because of the potential operational problems arising from the degradation of fuels when used to cool aircraft components. Within this program, investigations are proceeding to develop candidate advanced thermally stable fuels, kinetic models of fuel degradation and to measure parameters for computational fluid dynamic models to predict the degradation of fuel under various conditions. This report summarizes the development and testing of instrumentation systems to measure solid particle formation during fuel thermal stressing and to measure the accumulation rates of solids on a surface, and describes analyses of jet fuel liquids and formed solids.					
20. DISTRIBUTION / AVAILABILITY OF ABSTRACT <input checked="" type="checkbox"/> UNCLASSIFIED/UNLIMITED <input type="checkbox"/> SAME AS RPT. <input type="checkbox"/> DTIC USERS			21. ABSTRACT SECURITY CLASSIFICATION Unclassified		
22a. NAME OF RESPONSIBLE INDIVIDUAL William E. Harrison III			22b. TELEPHONE (Include Area Code) 513-255-6601	22c. OFFICE SYMBOL WL/POSF	

DISCLAIMER

This report was prepared as an account of work sponsored by the United States Government. Neither the United States nor any agency thereof, nor any of their employees, makes any warranty, express or implied, or assumes any legal liability or responsibility for the accuracy, completeness, or usefulness of any information, apparatus, product, or process disclosed, or represents that its use would not infringe privately owned rights. Reference herein to any specific commercial product, process or service by trade name, mark, manufacturer, or otherwise, does not necessarily constitute or imply its endorsement, recommendation, or favoring by the United States Government or any agency thereof. The views and opinions of authors expressed herein do not necessarily state or reflect those of the United States Government or any agency thereof.

Accession For	
NTIS GRA&I	<input checked="" type="checkbox"/>
DTIC TAB	<input type="checkbox"/>
Unannounced	<input type="checkbox"/>
Justification	
By _____	
Distribution/	
Availability Codes	
Dist	Avail and/or Special
A-1	



FOREWORD

In May 1989, the Fuels Branch of the Aero Propulsion Directorate at Wright-Patterson Air Force Base, Ohio, commenced an investigation to develop advanced, thermally stable jet fuels as well as physical and computer models that could simulate the thermal degradation of those fuels under operational conditions. Funding was provided to the Department of Energy (DOE) Pittsburgh Energy Technology Center (PETC) to administer this effort. This report, Volume 1 of 2 volumes, details efforts of Sandia National Laboratories (SNL), a prime contractor to DOE (DOE Contract Number DE-AC04-76DP00789). Development and testing of diagnostic instrumentation systems and analyses of jet fuel liquids and formed solids are described. Mr. William E. Harrison III was the Air Force Program Manager, Mr. Swenam Lee, Mr. Mike Baird, and Mr. Shelby Rogers were the DOE/PETC Program Managers, and Dr. Howard Stephens was the SNL Program Manager.

TABLE OF CONTENTS

	<u>Page</u>
I. INTRODUCTION	1
II. SYSTEM DEVELOPMENT AND TESTING	1
A. PARTICLE SIZE MEASUREMENTS	2
1. Test Cell Fabrication and Diagnostics	2
2. Development and Testing of Photon Correlation Spectroscopy System	3
Instrument Control and Size Distribution	9
Analysis Software	
Evaluation and Calibration of the PCS System	10
Experiments on Heated Particle Size Standards	10
3. Experiments on Heated Jet Fuel	13
Tests on Pre-stressed Samples	13
In Situ Thermal Stress PCS Measurements	14
4. Design of Pressure Vessel	17
B. MEASUREMENT OF DEPOSIT MASS ACCUMULATION	17
1. Investigation of Acoustic Devices for Monitoring Jet Fuel Degradation	18
Acoustic Plate Mode (APM) Device Operation	18
Results of APM Jet Fuel Tests	21
2. Quartz Crystal Microbalance (QCM) Operation	23
C. LIQUIDS AND SOLIDS CHARACTERIZATION STUDIES	31
1. Thermal Stress Tests on JP-8 Fuel	31
2. FTIR Analyses	35
3. Analyses of Afterburner Injector Arm and Deposits	35
III. CONCLUSIONS	43
REFERENCES	48

FIGURES

<u>Figure</u>	<u>Page</u>
1. Measured correlation function $G(\tau)$ for JP-8 at 110-120°C; Correlation is weak.	5
2. Measured correlation function $G(\tau)$ for JP-8 at 155-160°C; Correlation is well-defined.	6
3. Schematic layout of PCS system for studies of heated jet fuels. I1 and I2: Iris apertures; P1 and P2: pinholes; FL: focusing lens; CL: collection lens; EM: energy monitor; NBIF: narrow bandwidth interference filter; PMT: photomultiplier tube; HV: high voltage PMT power supply; A/D: signal amplifier/discriminator; LVPS: low voltage power supply.	8
4. Particle diameters measured by the dedicated PCS system vs. true particle diameter (manufacturer's specifications traceable NIST standards).	11
5. Size Distributions (as calculated by CONTIN) from two samples containing 20-nm and 105-nm Particles.	12
6. Post-test PCS analysis of JP-8 sample heated to 160°C. Analysis made at room temperature.	15
7. Schematic of an acoustic plate mode (APM) device showing the shear horizontal (SH) displacement of the mode. Each transducer consists of 75 interdigitated electrode pairs, (one is shown).	19
8. Cutaway view of acoustic plate mode (APM) sensor with teflon cell and reflux condenser.	20
9. APM frequency response vs. time during thermal degradation of 1.5 ml JP-8 and 0.015 ml EHA under flowing oxygen. The temperature of the runs were (●) 150, (■) 167, and (▲) 184°C.	22
10. Schematic of quartz crystal microbalance (QCM), consisting of circular electrodes patterned on both sides of a thinned AT-cut quartz disk.	24
11. Cross-sectional view of a QCM simultaneously loaded on one side by a mass layer and a contacting liquid.	25
12. The equivalent circuit for a QCM under mass and liquid loading including parasitic capacitance in the test fixture C_p .	27

FIGURES

<u>Figure</u>	<u>Page</u>
13. QCM admittance measured (points) and calculated (lines) near the fundamental resonance as the density-viscosity product ($\rho\eta$, $\text{g}^2/\text{cm}^4\text{-s}$) of a contacting fluid increases: (A) air, $\rho\eta = 2 \times 10^{-7}$; (B) water, $\rho\eta = 0.010$; (C) 43% glycerol in H_2O , $\rho\eta = 0.044$; (D) 64% glycerol in H_2O , $\rho\eta = 0.15$; (E) 80% glycerol in H_2O , $\rho\eta = 0.72$.	28
14. QCM admittances measured (points) and calculated (lines) before and after deposition of a 124 nm Au layer. Before Au deposition: (A) in air, (B) in water; after Au deposition: (C) in air, (D) in water.	29
15. Test fixture that uses a QCM to monitor jet fuel properties at elevated temperatures. A temperature controller uses thermocouples to measure chamber temperature and regulates power to the band heater to maintain a preset temperature.	30
16. QCM admittance measured (points) and calculated (lines) before and after immersion in JP-8 jet fuel at 20°C . The viscosity-density product calculated from the curve for the jet fuel is indicated.	32
17. Raman spectra of injector arm: 0.0, 0.5, and 2 cm from tube end.	38
18. Raman spectra of injector arm: 10.5 cm from tube end.	39
19. Raman spectra of injector arm: 2.0, 9.0, 10.5, and 13.2 cm from tube end.	40
20. Raman spectra of injector arm: 11.5, 12.0 and 13.2 cm from tube end.	41
21. Raman spectra of injector arm: 11.5 and 13.2 cm from tube end; no background correction.	42
22. Raman spectra of injector arm (13.2 cm from tube end) compared with carbonization from JP-8 fuel stressed at 550°C .	44
23. Raman spectra of carbonization from JP-8 fuel stressed at 550°C in air at 100 psi and at 800 psi.	45
24. Raman spectra of amorphous deposits from injector arm and carbonization from JP-8 fuel stressed at 550°C .	46

TABLES

<u>Table</u>	<u>Page</u>
1. Analyses of PCS Measurements Using MARLIN.	10
2. Analyses of PCS Measurements of 105-nm Particles at 24°C, 45°C, and 56°C.	13
3. Analyses of PCS Measurements Using MARLIN, EXSAMP, and CONTIN.	14
4. Analyses of PCS Measurements on Jet A-1 Heated to 170°C.	16
5. Summary of Results of APM Studies of Surface Deposition Caused by Thermal Degradation of JP-8 Jet Fuel.	21
6. JP-8 Thermal Stress Test Matrix and Observations.	33
7. Gas Analyses on Jet Fuel JP-8 Tubing Bomb Thermal Stress Tests (All tests performed for 1 hr under 300 psi air).	34
8. Typical Carbon-Hydrogen-Nitrogen Compositions of Deposits from Afterburner Injector Arm.	36

Acknowledgements

This Project was jointly supported by the U.S. Department of Energy, Pittsburgh Energy Technology Center (PETC) and the Aero Propulsion and Power Directorate, Wright-Patterson AFB, OH. This work was supported by the U.S. Department of Energy at Sandia National Laboratories under contract DE-AC04-76DP00789. The authors wish to express their appreciation to Messrs. S. Lee, M. Baird, and S. Rogers (PETC) and Mr. W. E. Harrison III and Dr. W. M. Roquemore (Aero Propulsion and Power Directorate) for their support of this effort. The authors would also like to acknowledge R. J. Kottenstette, H. P. Stephens, L. V. Salgado, D. M. Haaland, A. S. Geller, G. C. Nelson, D. Tallant (Sandia National Laboratories) for their technical support.

I. INTRODUCTION

Thermal stability of aviation fuels is of concern because of the potential operational problems arising from fuel degradation under thermal stress conditions. Hydrocarbon fuels in contact with heated metallic surfaces form insoluble, carbonaceous deposits that can foul nozzles, manifolds, filters, injectors, and heat exchangers. Temperatures in current aircraft reach approximately 163°C (325°F); temperatures in future aircraft, with expected speeds above Mach 4, are expected to reach over 627°C (1160°F). The methods of dissipating the large heat loads will be one of the key factors in determining the capabilities of future aircraft. The use of heat exchangers in which the fuel is used as the primary or secondary coolant appears to be an effective way of dissipating heat. While currently used jet fuels are thermally stable within present aircraft operational limits, the anticipated increases in the thermal loading applied to fuel systems of high-performance aircraft have prompted the development of advanced, thermally stable aviation fuels and methods to predict the stability of these fuels under varying operating conditions.

A long-term effort to develop thermally stable fuels for aircraft was initiated in FY89 by the U.S. Air Force, working jointly with the Department of Energy, Pittsburgh Energy Technology Center [1]. Sandia National Laboratories, Albuquerque, is the lead laboratory within the Advanced Thermally Stable Jet Fuels Development Program in conducting efforts to (1) develop candidate advanced, thermally stable fuels and kinetic models for their thermal degradation and (2) develop the capability to predict the fuel thermal stability (i.e., the amounts, characteristics, and locations of solid deposits) under given operating conditions. Investigations to support these objectives include studies of model compounds and mixtures representative of petroleum- and coal-derived fuels to correlate thermal stability with composition and determine reaction mechanisms; those investigations are reported in Volume II of this annual report. This document discusses instrumentation and apparatus developed and used to measure parameter values associated with the formation and deposition of solids from decomposition of hydrocarbon jet fuels. Results of initial tests are presented. Data obtained from these tests will be used to develop physical and mathematical models for the prediction of fuel thermal stability under given operation conditions.

II. SYSTEM DEVELOPMENT AND TESTING

Model development for the coupled flow, heat transfer, mass transport, and chemical processes occurring in an aviation fuel system requires measurement of fluid velocities, temperatures, and physical and chemical characteristics of the liquid- and solid-phase reactants and products present during the fuel degradation and solids deposition process. Instrumentation techniques for measurement of parameters related to hydrocarbon fuel thermal stability were evaluated and developed for use in

performing both static and dynamic tests of fuel stability. Based upon tests and evaluations performed during the first year of the project [1], various techniques were identified to measure physical and chemical parameter values; two techniques were identified as requiring more extensive development for use in jet fuel thermal stability tests. The development and testing of these techniques, a particle size measurement system and a mass accumulation sensor system, were the focus of study during the preceding year and are described in detail. Additional liquid-phase and solid-phase characterization studies were performed and results are presented.

A. PARTICLE SIZE MEASUREMENTS

Particle size formation and growth during hydrocarbon thermal degradation has been identified as a potentially important mechanism in the formation of deposits [1]. During this reporting year, a system for measuring particle size distributions, photon correlation spectroscopy, was developed and preliminary testing completed. Testing of jet fuel is planned at elevated temperatures at ambient and above-ambient pressures. The fabrication of a pressure vessel was completed that will enable testing at temperatures up to 1000 K and over 1100 psig. The following sections discuss the fabrication, testing, and diagnostic evaluation of sample cells, development and testing of Photon Correlation Spectroscopy (PCS) system, performing PCS measurements on jet fuel samples during thermal stress tests, and the design and operation limits of the pressure vessel.

1. Test Cell Fabrication and Diagnostics

Performance evaluation continued on the static thermal cell (quartz cube and copper heater). Static thermal stress testing was used to study the fuel degradation process without flow. A prototype thermal cell consisting of a quartz cube and a heater enclosure was constructed. Two different sized quartz cubes were manufactured at Sandia. The first quartz cube had sides of 7.6 cm each, while the second was 3.8 cm on a side. The method for fabrication of these cells has been developed so that cells of smaller size and varying geometries can be produced. Assembly of the heater enclosure was completed and also has a cubic geometry. The heater encapsulates the quartz cubes and heats the fluid contained in the quartz cubes to the desired temperature. The heater enclosure is manufactured of 0.635-cm-thick copper plate to minimize temperature distributions and has grooves machined into the plates to facilitate two 0.318-cm-diameter heaters.

Preliminary evaluation of the thermal cell assembly has included measurement of the heater wall and liquid bulk temperature uniformity and heating rate. Both the 7.6-cm and 3.8-cm square cells have been tested in the heater assembly. Optical access to the quartz cells is provided through quartz windows in the heated copper walls. Tests to date have

used water as the heated liquid, and have been performed at atmospheric pressure, limiting maximum liquid temperature to about 95°C to prevent excessive boiling. The heater wall and liquid heating rates and maximum temperatures for various electrical power inputs were determined using arrays of thermocouples. The liquid temperature always lags the wall temperature. The smaller liquid volume in the 3.8-cm cell allows considerably faster heat up. Measured liquid temperatures in the small cell are uniform to within 0.5°C. The cell/heater assembly was designed to be integrated with the PCS system and other diagnostic instrumentation for later fuel thermal stress tests.

An alternate design, a smaller heater/cell holder, was assembled and is being used for preliminary in situ jet fuel thermal stress/PCS tests. This device consists of cylindrical copper shells that slide tightly over the top and bottom of the 25-ml cylindrical glass cells currently used for PCS static tests. Heating tapes are wound tightly around these copper shells, and the heating tapes are controlled by a thermocouple feedback unit which can be set to maintain the fuel at a constant setpoint temperature. Type K thermocouples are positioned at the glass/copper interface to determine the maximum temperature seen in the fuel sample, and in the center of the cell (submerged) to measure the temperature at the location of PCS measurements. The submerged thermocouple is used as the input for the heater feedback controller. The maximum heat input is 160 W, and this device has been used to heat Jet A-1 as high as 250°C. The temperature at the measurement location is held constant to within about ±2% of the setpoint temperature. Additional tests will incorporate additional submerged thermocouples in order to determine precisely the temperature at the PCS measurement location (needed for accurate viscosity determination) and to determine the magnitude of temperature gradients in the sample cell.

2. Development and Testing of Photon Correlation Spectroscopy System

Photon correlation spectroscopy (PCS) is a laser-based, dynamic light scattering technique for measuring particle diffusion coefficients, which are then used to determine particle sizes in the 3- to 10000-nanometer-diameter range. Preliminary studies of JP-8 and JP-8X samples have shown that PCS is a useful technique for measuring particle growth in thermally stressed jet fuels [1]. The capability for accurate small particle sizing is particularly important since much of the relevant fuel degradation chemistry occurs in a regime where particle diameters are generally less than 100 nm [2]. These studies (using commercial and research PCS devices developed for other projects at Sandia) demonstrated a systematic trend of particle growth with increased exposure of fuel samples to elevated temperatures. PCS provides the capability for noninvasive, in situ measurements of time-dependent particle size distributions in heated fuels under ambient or high-pressure conditions. A PCS system for these measurements was designed and assembled, and experiments performed using model systems and jet fuel.

PCS works by measuring the time-dependent intensity of the scattered light signal caused by Brownian motion of the particles in an illuminated sample. Large particles produce low frequency oscillations in the scattered signal, and small particles produce high frequency oscillations. A laser beam is focused into the sample of interest and a photomultiplier is used to collect the light scattered at some angle. The photomultiplier output signal $I(t)$, the fluctuating intensity signal, is processed by a digital correlator, which performs an autocorrelation of the intensity fluctuation signal

$$G(\tau) = \langle I(t)I(t+\tau) \rangle. \quad (1)$$

where $I(t)$ and $I(t+\tau)$ are the intensity at times t and $t+\tau$, respectively. For a monodisperse suspension of particles

$$G(\tau) \propto e^{-2\Gamma\tau}, \quad (2)$$

where the exponential decay constant Γ (gamma) can be expressed as

$$\Gamma = Dq^2, \quad (3)$$

where D is the diffusion coefficient, and q the scattering wave vector

$$q = 4\pi\eta \sin(\theta/2)/\lambda_1, \quad (4)$$

with η the liquid refractive index, θ the scattering angle, and λ_1 the incident laser wavelength. Particle size is determined using the Stokes-Einstein equation

$$D = k_B T / (3\pi\eta d), \quad (5)$$

where k_B is the Boltzmann constant, T the absolute temperature, η the fluid viscosity, and d the particle diameter. Figures 1 and 2 are two examples of autocorrelation functions $G(\tau)$, both collected during in-situ thermally stressed JP-8 experiments. Unstressed fuel samples to date have exhibited no correlation, indicating that very few particles are present. As the fuel is heated, at some critical temperature weak correlation becomes evident, as shown in Figure 1 (fuel temperature approximately 110°C-120°C). At higher temperatures, the correlation becomes more well-defined and simpler to analyze with the software routines described below. Figure 2 presents an example of such a strong correlation, this one for JP-8 at approximately 155°C-160°C.

PCS is performed with a relatively simple optical setup. Detailed discussions of instrumentation and data reduction methods are available [3,4]. Briefly, a vertically polarized laser beam is focused into the sample of interest and a photomultiplier is used to detect the dynamic behavior of the scattered light signal. The photomultiplier output is fed to an amplifier/discriminator to produce a uniform series of pulses with

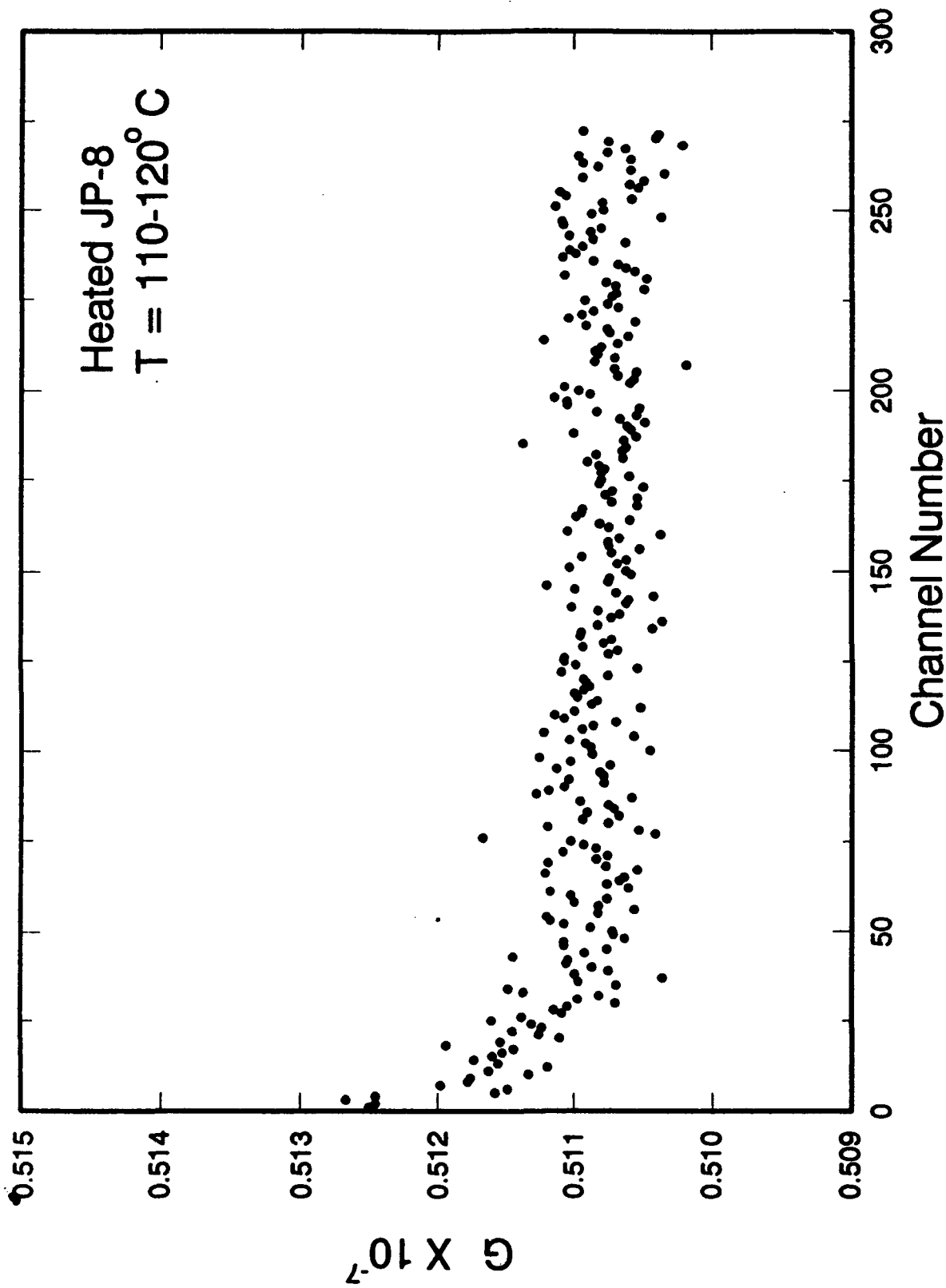


Figure 1. Measured correlation function $G(r)$ for JP-8 at 110-120°C; Correlation is weak.

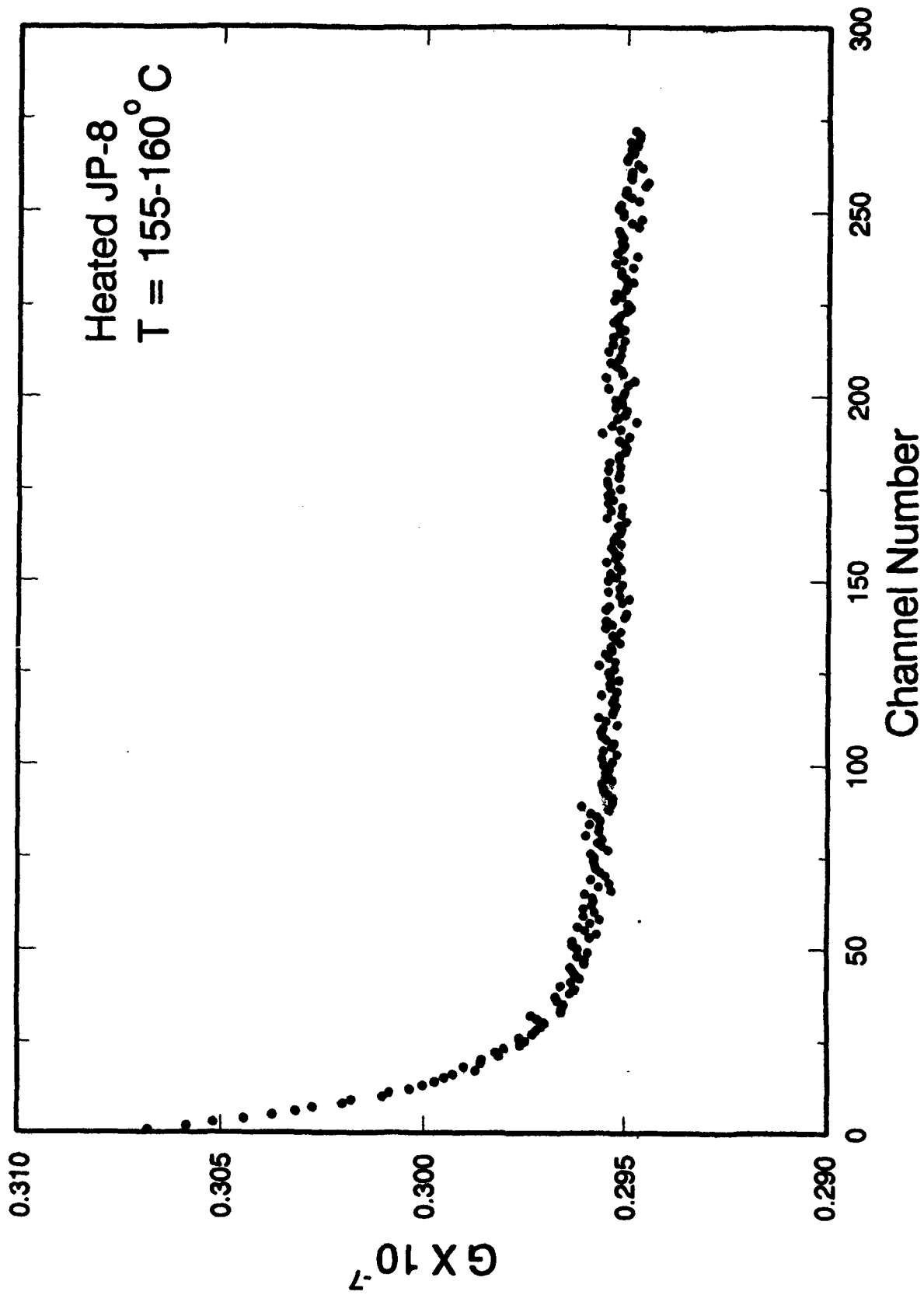


Figure 2. Measured correlation function $G(r)$ for JP-8 at 155-160°C;
Correlation is well-defined.

variable interpulse periods. This signal is sent to a digital correlator which performs the autocorrelation.

Successful application of PCS to a system containing an unknown distribution of particle sizes frequently requires measurements at two or more scattering angles [5]. For the PCS system assembled for this project, this was accomplished by mounting the photomultiplier on an optical rail that rotates about the sample cell while maintaining a fixed geometry between the input laser beam and sample. A computer-controlled goniometer is used to determine precisely the angle of rotation.

Several other items were implemented to permit quantitative PCS measurements. A system of pinholes is used to define the area over which the phase of scattered light is correlated. For a two-pinhole arrangement, optimum detection is obtained when the following criterion is met:

$$(d_{p1} \times d_{p2})/\lambda_0 L = 1 \quad (6)$$

where λ_0 is the wavelength of scattered light, d_{p1} and d_{p2} are the diameters of the first and second pinholes, respectively, and L is the distance between them (see Figure 3). Moreover, a frequency counter is available to ensure that the total photon count rate is maintained below 10 MHz [5]. This item is also useful in optimizing the alignment of the sample and detection system. Finally, a power meter is used to monitor the laser output and to determine light extinction in the sample.

Assembly of the dedicated PCS assembly was completed in October 1990. A schematic diagram of the experimental assembly is shown in Figure 3. Items that facilitate computer control of the experiment have been obtained in order to simplify data acquisition and enhance the portability of the PCS system. The various components of the system were described in detail in [6].

In initial tests, problems with the photodetection instrumentation of the PCS system were encountered. However, these problems have been resolved. The PMT and amplifier/discriminator are currently operating with low noise and without anomalous bursts of high signal. A spare PMT and a second amplifier/discriminator have been received and are available, if needed. A high-voltage power supply specifically designed for use with PMT's (EG&G Ortec Model 556H) has been installed. For nearly "dust-free" samples, the observed count rates are consistently stable to within a few percent.

In response to the results from the initial tests, the PCS system collection optics were modified to include: (1) a shorter focal length (5 cm) lens to improve the collection efficiency and (2) an imaging microscope to view the scattering volume and aid in the alignment of the lens and pinholes. The microscope assembly was rigidly mounted (along

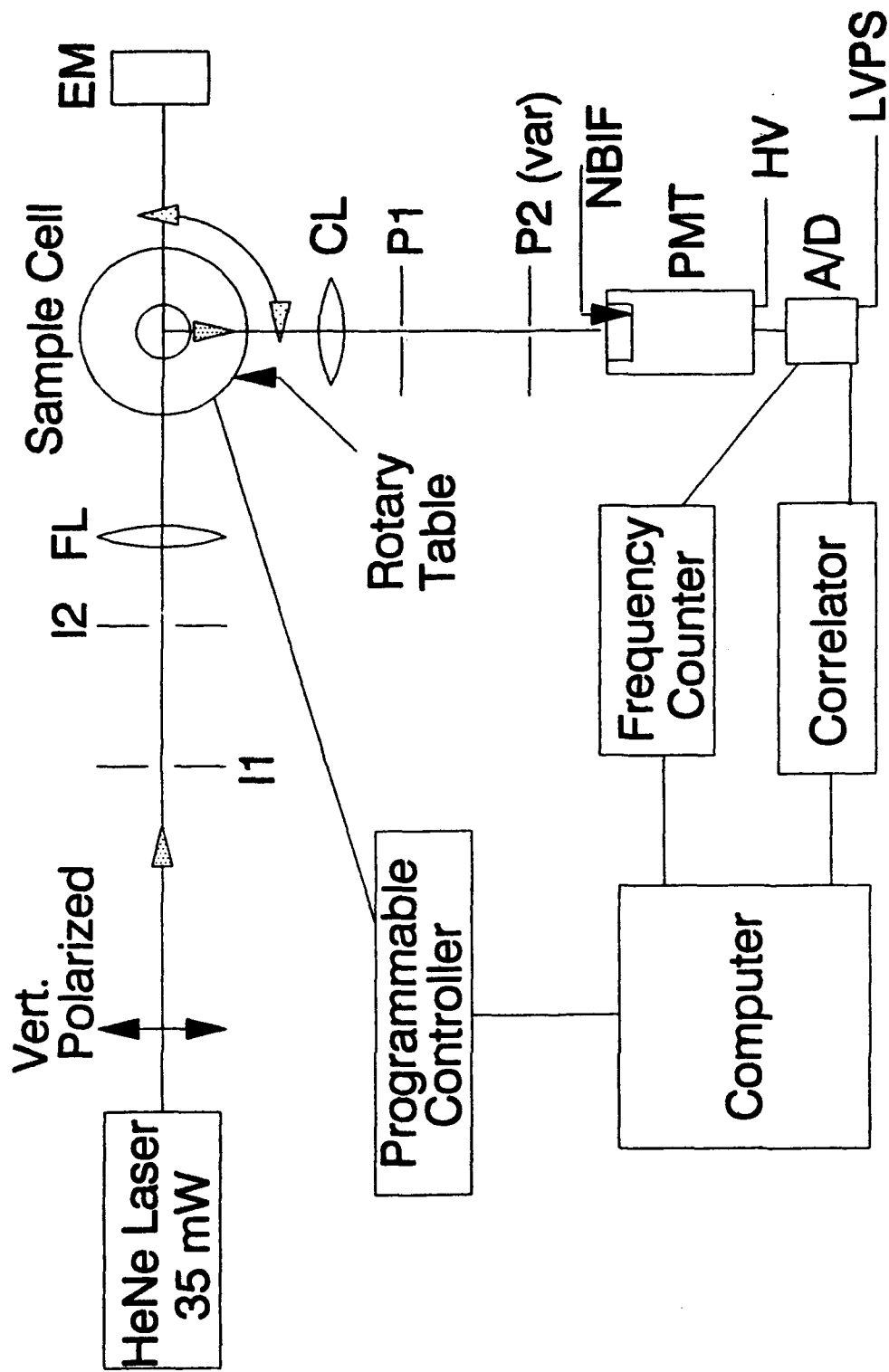


Figure 3. Schematic layout of PCS system for studies of heated jet fuels. I1 and I2: Iris apertures; P1 and P2: pinholes; FL: focusing lens; CL: collection lens; EM: energy monitor; NBIF: narrow bandwidth interference filter; PMT: photomultiplier tube; HV: high voltage PMT power supply; A/D: signal amplifier/discriminator; LVPS: low voltage power supply.

with the second pinhole) to the PMT housing. A rotating mirror allows the scattered laser light to be directed to the PMT or microscope optics, as desired. The microscope is used to examine the PCS system coherence area (essentially the diffraction pattern of the scattering volume) as well as for alignment.

Experiments on samples with a wide range of particle diameters have demonstrated the utility of variable apertures at both pinhole locations in the PCS system. Pinholes from 0.05-mm to 5-mm diameter have been ordered. These items will be installed in Spindler & Hoyer Model 03-6121 rotating mounts to facilitate "in-line" optimization of both apertures.

Instrument Control and Size Distribution Analysis Software

With the AN01 option (an "add-on" IC that performs first and second cumulants analysis of the correlation waveform) on the LFI 1096 digital correlator, the mean size of a simple monomodal particle distribution can be obtained directly. However, on the basis of previous measurements on jet fuels, we anticipated that fairly complex distributions of particle sizes may be observed. In particular, "dusty" samples may be encountered under certain conditions. Hence, it is important to have a satisfactory array of software routines for analysis of unknown samples. A flexible and robust package of instrument control and size distribution analysis software for dynamic light scattering studies was obtained from Dr. Paul Russo (Department of Chemistry, Louisiana State University, Baton Rouge, LA). This package is designed for use with the LFI 1096 digital correlator and an IBM PC-type host computer [7].

As received, the software includes the following modules: LFI232 (for communication and data transfer between the LFI 1096 and computer on the RS232 line), SIMDATA (a raw data simulation routine for program evaluation), CORAN (a 1st to 3rd order cumulants analysis routine for data screening and summation), MARLIN (a discrete exponential fitting program), EXSAMP (a rapid, smoothed algorithm for Laplace inversion of the first order autocorrelation function), and the "state-of-the-art" CONTIN Laplace inversion routine. The package also contains a variety of programs for generation of screen printed and hardcopy plots. With a 386-type computer and corresponding math coprocessor, the typical run time for the largest program is less than 5 minutes.

The LFI232 program for communication and data transfer between the digital correlator and host computer was tested and verified for our set-up. In addition, we have examined the analysis routines on simulated and real data for a wide range of conditions [6,9]. The available array of flexible and complementary analysis programs is an important asset in the characterization of jet fuel samples with unknown particle size distributions.

Evaluation and Calibration of the PCS System

To characterize and calibrate the dedicated PCS system, monodisperse and bimodal samples of polystyrene spheres suspended in aqueous solution (Duke Scientific, Palo Alto, CA) were examined. Figure 4 illustrates results from monomodal samples with particles in the 20-500-nm-diameter range. Most samples were contained in standard cylindrical test cells; however, the quartz Thermal Stress Cell (1.5-inch cube) was used for some measurements on 105-nm-diameter particles. Fairly accurate sizing was obtained over the entire range; a substantial part of the "scatter" in the data can be attributed to some uncertainty in the sample temperature and viscosity (near room temperature the viscosity of water varies by over 2 percent per degree). For the larger diameters, evidence of number fluctuation problems [8] was also seen. These effects can be minimized by varying the focal length of the focusing lens and/or pinhole sizes.

Measurements on mixtures of 20-nm and 105-nm particles were also successful. Data from two samples have been analyzed in detail. In preparation of these samples, no attempt was made to control precisely the concentrations of the two particles; however, one sample (Sample 2) contained approximately twice the number of 20-nm particles as the other (Sample 1). Fits from MARLIN (a discrete exponential fitting program) [4] were obtained as shown in Table 1.

Table 1. Analyses of PCS Measurements Using MARLIN

	<u>MARLIN (Sample 1)</u>	<u>MARLIN (Sample 2)</u>
Amplitude (1)	0.039	0.069
Amplitude (2)	0.961	0.931
Diameter (1, nm)	25.2	18.5
Diameter (2, nm)	107.2	105.7

The diameter obtained for the larger component is in excellent agreement with the manufacturer's specifications. The experimentally determined size of the smaller component is also reasonably good considering the small amplitude. The distributions calculated by CONTIN (a Laplace inversion routine) are shown in Figure 5. For Sample 2, both components were resolved and sized with fair accuracy.

Experiments On Heated Particle Size Standards

Preliminary experiments on heated samples of 105-nm particles in aqueous solution have been conducted. In one case, the sample was heated to 56°C at a rate of approximately 5 degrees per minute. PCS measurements were taken at three temperatures: 24°C, 45°C and 56°C. The fits from MARLIN are shown in Table 2.

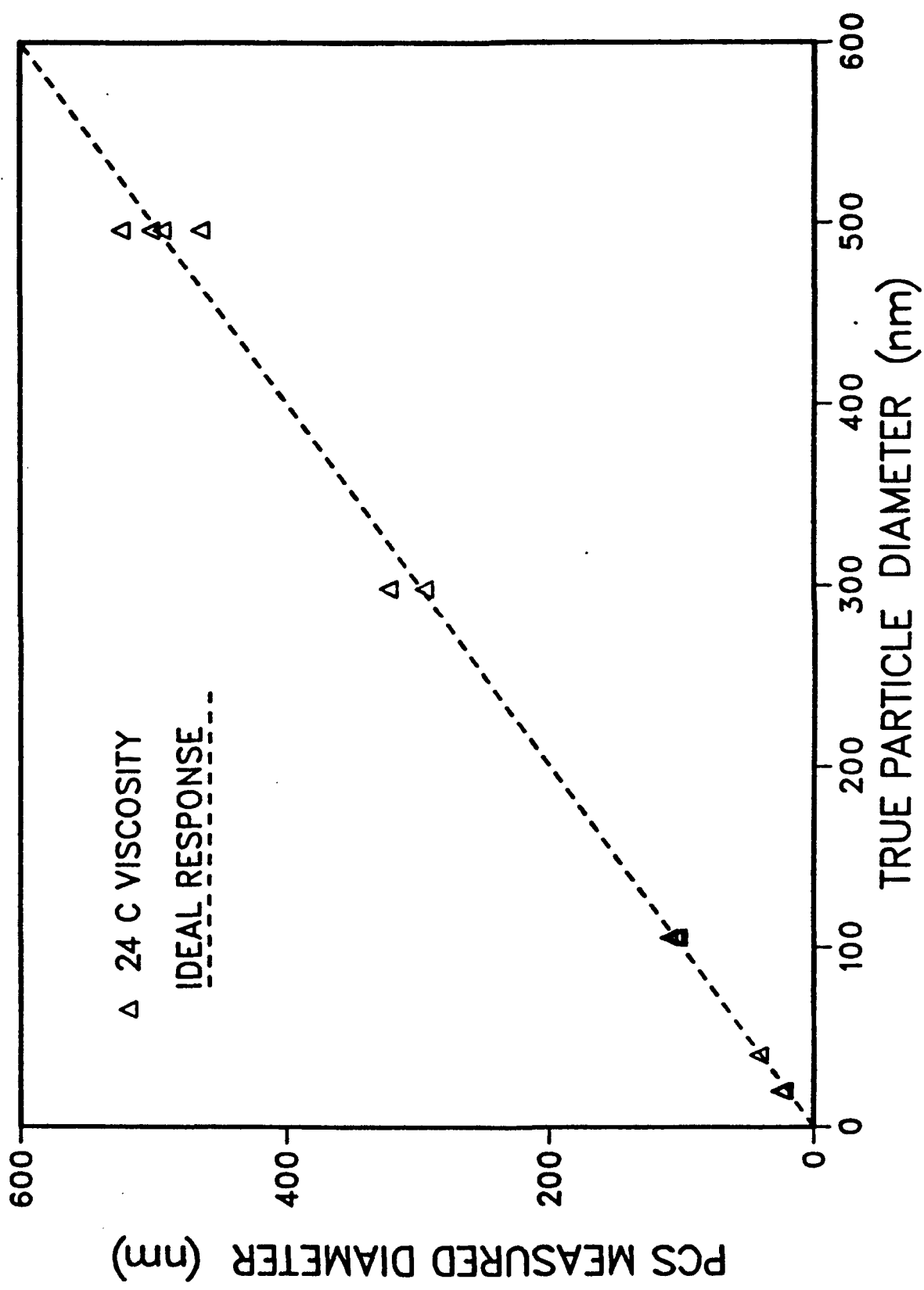


Figure 4. Particle diameters measured by the dedicated PCS system vs. true particle diameter (manufacturer's specifications traceable NIST standards).

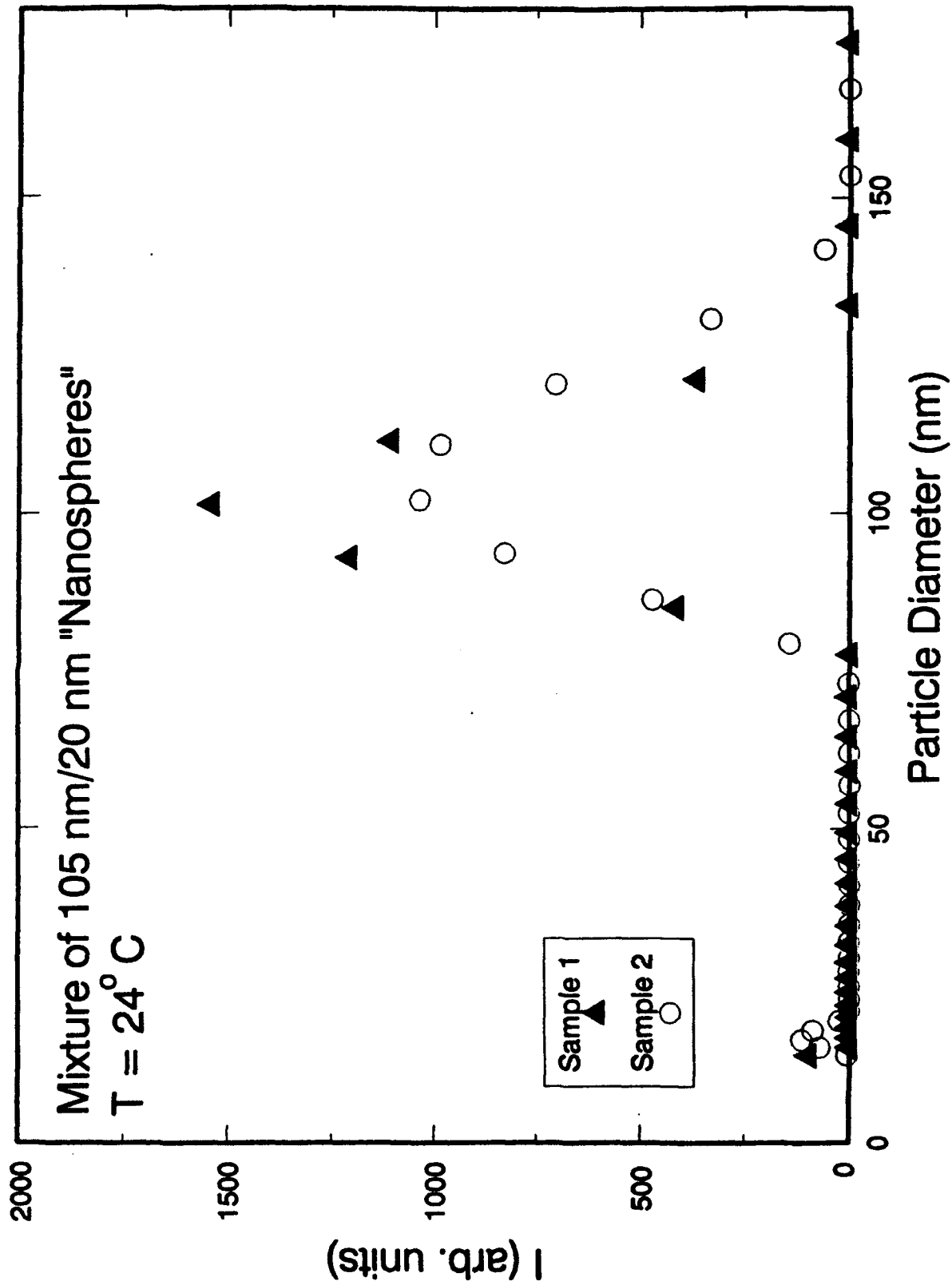


Figure 5. Size Distributions (as calculated by CONTIN) from two samples containing 20-nm and 105-nm Particles.

Table 2. Analyses of PCS Measurements of 105-nm Particles at 24°C, 45°C, and 56°C.

	<u>T = 24°C</u>	<u>T = 45°C</u>	<u>T = 56°C</u>
Gamma (Hz)	1508.7	2477.2	3096.5
Diameter (nm)	110.9	111.7	110.0

The distribution determined by CONTIN for the sample at 45°C indicates a calculated diameter is 106.3 ± 7.2 nm, in excellent agreement with the known size. The CONTIN distribution also contains a very small amplitude component at larger diameter (possibly because of dust in the sample). The primary effect observed in these tests was the substantial variation in the decay rate (i.e., Gamma) of the first order correlation function as a function of temperature and viscosity. Accurate particle sizing requires a knowledge of both parameters--a factor that is very important in studies of heated jet fuels and model compounds. Perturbations that are due to sample convection, etc. were negligible for these tests.

Programmatic needs require particle detection and accurate sizing over a wide range in heated jet fuel samples. The system evaluation tests and the tests in heated samples indicate that the PCS system can provide these measurements.

3. Experiments On Heated Jet Fuel

The PCS system was used for room temperature analysis of pre-stressed JP-8 fuel samples and for in situ tests of heated JP-8 and Jet A-1 samples. Those experiments indicate that processes leading to particle formation in heated fuels are complex and sensitive to initial fuel composition as well as heating rate and temperature, particularly in the range 100°C-180°C.

Tests on Pre-stressed Samples

Room temperature measurements were made on JP-8 fuel that had been placed in a 30-ml reactor made of 316 stainless steel and heated to various temperatures by immersion in a sand bath. The maximum temperature applied to the individual samples ranged from 160°C to 398°C. Best results were achieved with the fuel exposed to 160°C. Visual inspection of this stressed sample showed that the fuel was slightly darker in color than the neat fuel; however, the sample was relatively free of dust and sediment. Very strong scattered laser intensity was observed at a 90-degree scattering angle and PCS measurements indicated a simple, nearly monomodal distribution of particle sizes. Fits from MARLIN, EXSAMP, and CONTIN were obtained and are shown in Table 3.

Table 3. Analyses of PCS Measurements Using MARLIN, EXSAMP, and CONTIN

	<u>MARLIN</u>	<u>EXSAMP</u>	<u>CONTIN</u> <u>(chosen fit)</u>
Diameter (nm):	282	297 ± 62	279 ± 19

The distribution determined by CONTIN is shown in Fig. 6. This calculated distribution exhibits a small amplitude component at diameters >1 micron, a result that was evident in results of the other two algorithms as well. The formation of a substantial concentration of relatively large particles under these test conditions is consistent with previous measurements on JP-8 stressed at 185°C under 300 psi air [1].

Results for fuel pre-stressed to T = 180°C and higher were more ambiguous. Many of these samples contained significant quantities of dust and sediment. Without additional sample preparation, these conditions made it difficult to obtain meaningful correlations even though strong scattered light signals were observed in all cases. In general, the correlation functions exhibited at least two components, suggesting particle distributions with average sizes on the order of hundreds of nanometers and >> 1 micron, respectively. For the 180°C sample, consistent results were obtained for the average size of the smaller component as follows:

	<u>MARLIN</u>	<u>CONTIN (chosen fit)</u>
Diameter (nm):	446	416 ± 45

In Situ Thermal Stress PCS Measurements

For the in situ measurements, some samples have been prepared using repeated filtration (10-micron pore size) while others have utilized the fuels as supplied. Both JP-8 and Jet A-1 fuels contain sufficient numbers of dust particles to complicate acquisition of the correlation function at small scattering intensities. With filtration, nearly dust-free (i.e., easily analyzed) samples could be generated; however, the possible effects of this sample preparation step on the overall particle formation process (during heating) have not been characterized. Thus far, no attempt has been made to maintain or boost the oxygen content of the fuels during stress testing.

Clearly, processes occurring at T < 160°C are important in defining the early stages of particle formation. Accordingly, we have concentrated on this temperature regime in initial real-time, in situ studies of heated fuels. Two principal effects have been monitored as a function of temperature: (1) changes in the intensity of scattered laser light and (2) the evolution of the autocorrelation function. At temperatures as low

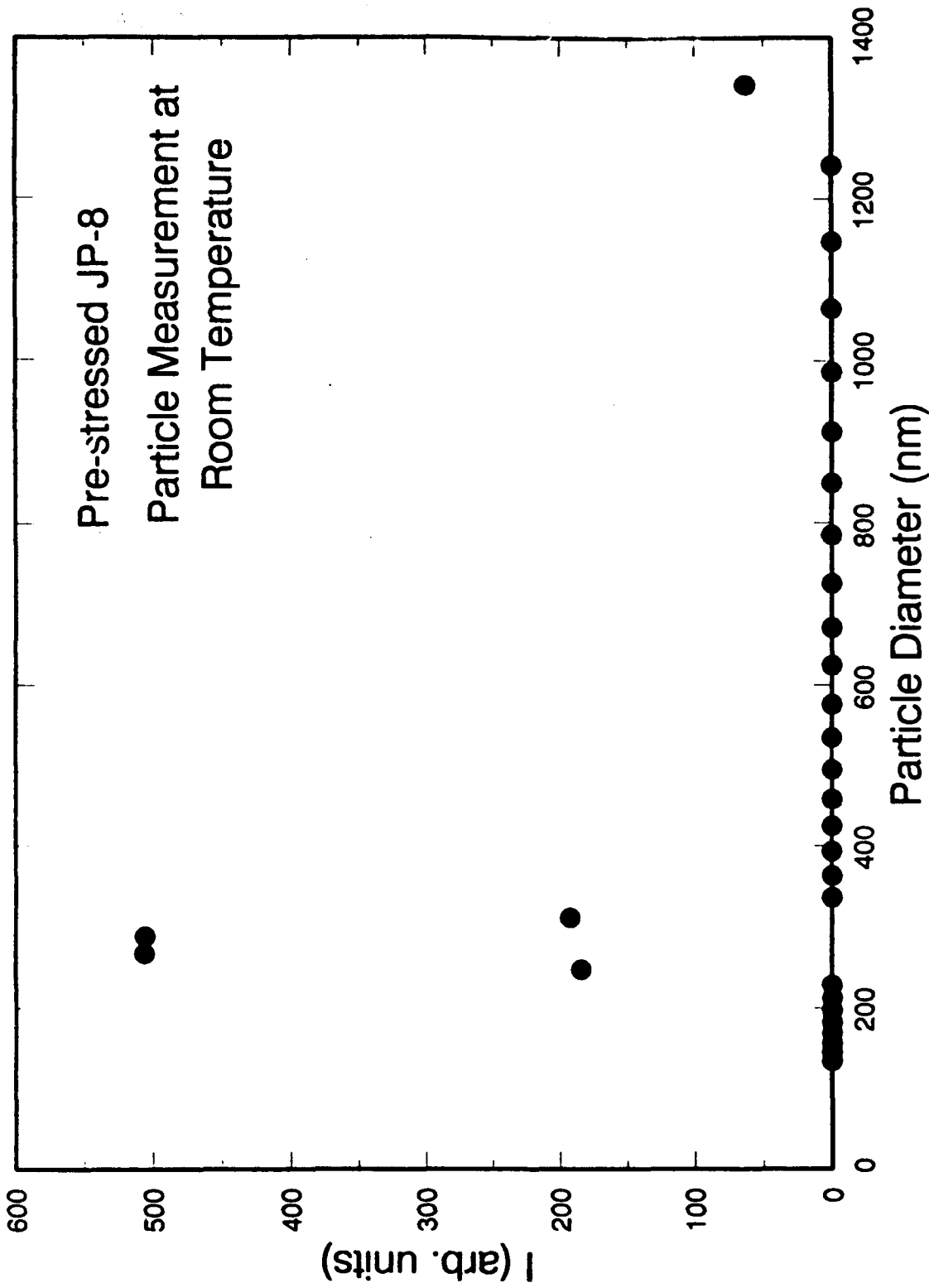


Figure 6. Post-test PCS analysis of JP-8 sample heated to 160°C. Analysis made at room temperature.

as 80°C, a significant increase in the intensity of scattered light has been observed. A gain of up to a factor of two in signal intensity has been seen at temperatures approaching 175°C. Typically, the enhanced scattering intensity is "permanent;" i.e., it persists when the fuel cools to room temperature. This effect occurs in conjunction with particle formation in the sample and deserves more detailed analysis.

As mentioned in Section 2, a discernible decay rate in the autocorrelation function has been observed at fuel temperatures as low as 110°C (cf. Fig. 1). This condition corresponds to particle formation with a rather poorly defined size distribution. We have found that the temperature at which weak correlation is first observed can vary from sample to sample. Thus far, it appears that the scattered light intensity is a more sensitive indicator of early particle formation than the autocorrelation. In tests where Jet A-1 samples were heated to 125°C (2 hours at maximum temperature) and 145°C (1 hour at maximum temperature), respectively, we observed the usual enhancement in scattering intensity but little or no correlation. After cooling to room temperature, both samples displayed definite decay rates in the autocorrelation function, indicating a coalescence of size distribution around a well-defined average diameter. To sort out the various effects in the low-temperature regime, more careful control of experimental conditions (heating rate, temperature stability, temperature gradients in the sample cell, oxygen content in the fuel, etc.) and added sensitivity to small particle formation (by optimizing the collection optics and increasing the focused laser intensity) are required.

At temperatures near 160°C, a smooth autocorrelation function is consistently obtained (cf. Fig. 2). Analysis of real-time data acquired under these conditions yields a well-defined particle size distribution. For example, the fits obtained for a Jet A-1 sample heated to 170°C are shown in Table 4.

Table 4. Analyses of PCS Measurements on Jet A-1 Heated to 170°C.

	MARLIN	CONTIN (chosen fit)
Amplitude (1)	0.698	0.68
Amplitude (2)	0.302	0.32
Diameter (1, nm)	216	212 ± 21
Diameter (2, micron)	56	> 18

The average diameter of the smaller component is consistent with room temperature analysis of fuel samples pre-stressed to similar temperature levels.

Other thermal stress tests performed in which PCS measurements were obtained indicate that the particles are generally in the range in which this technique can obtain data relevant to the degradation and deposition

mechanisms. The initial set of measurements have shown that these mechanisms are sufficiently complex to preclude, at this time and with the small amount of data available, development of physical and mathematical models of particle formation and growth. For example, measurements obtained from stressing fuel that had been affected by storage (as noted by a slight discoloration of the fuel) differed from measurements of newly-received jet fuel of the same type. The matrix of future tests are designed to support development of the physical, and subsequently, mathematical models. Because the initial results suggest that measurement large particles ($>10 \mu\text{m}$) may be required, the PCS system is expected to be modified to permit these measurements and data analysis.

4. Design of Pressure Vessel

Construction of the "Thermal Stress Cell" (TSC) designed for jet fuel thermal stability tests was completed. The TSC was designed to operate at pressures up to 6.9 MPa (1000 psi) while containing fuel at temperatures up to 1000 K. The design consists of a pressure chamber, a thermal cell, and a heater assembly. The pressure chamber was manufactured of SCH-160, A-106 steel (Grade B, seamless) pipe 61 cm in diameter and 66 cm long and has maximum operating pressure and temperature of 10.3 MPa (1500 psi) and 550 K, respectively. Two 600 pound, 61-cm-diameter slip-on flanges (SA105 steel) were welded to the steel pipe and 600 pound blind flanges bolted to these flanges to complete the enclosure. Seven 7.6-cm-diameter, 900-pound flanged port penetrations were welded to the vessel to facilitate optical measurements, thermocouple and pressure measurements, power connections for heaters, inlets and outlets for flowing tests, etc. All welds were dye-penetrant tested to ensure integrity and painted to prevent rusting. Arrangements were made for hydrostatic pressure testing of the outer pressure chamber of the Static Test Cell. The maximum allowable working pressure has been set at 1176 psia, based on an anticipated maximum operating pressure of 1000 psia. Accordingly, hydrostatic testing will occur at a level of 1765 psia (1176 X 1.5).

B. MEASUREMENT OF DEPOSIT MASS ACCUMULATION

Measurement of the rate at which solids deposit on a surface has been identified as an important part of developing quantitative models to predict fuel thermal stability. Initially, an acoustic plate mode (APM) device was developed for monitoring solid deposition from jet fuel degradation. Because of operational problems involving the integrity of seals in the apparatus at elevated temperatures, a system utilizing a quartz crystal microbalance (QCM) was developed. This device has deposition-monitoring capabilities similar to the APM device, as well as a similar theoretical basis, but is more robust at elevated temperatures. The following sections discuss investigations performed with each device.

1. Investigation of Acoustic Devices for Monitoring Jet Fuel Degradation

Two types of acoustic devices have been investigated as potential monitors for jet fuel degradation. Both devices can be operated in contact with liquid and are very sensitive to surface mass changes. They thus have the potential to measure the accumulation of jet fuel degradation by-products on the device surface. Each device has advantages and disadvantages.

Acoustic Plate Mode (APM) Device Operation.

The acoustic plate mode (APM) device uses a thinned quartz plate as an acoustic waveguide, utilizing the propagating acoustic plate modes to probe the accumulation of surface mass. The device has interdigital electrodes photolithographically patterned on one surface of the quartz to excite and detect APMs in the thinned plate (see Figure 7). Since the modes have equal displacement on both sides of the plate, sensing may be performed on the side opposite the transducers. The excited modes have particle displacement parallel to the plane of the surface and thus continue to propagate efficiently when liquid contacts the device.

The accumulation of surface mass on the APM device causes the wave propagation velocity v to be decreased in proportion to the mass deposited:

$$\Delta v/v_0 = -c_m \rho_s \quad (7)$$

where v_0 is the unperturbed plate mode velocity, $c_m = 19 \text{ cm}^2/\text{g}$ is the mass sensitivity, and ρ_s is the mass density (mass/area) accumulated on one face.

When the APM sensor is incorporated as the feedback element of an oscillator loop, changes in propagation velocity are reflected as proportional changes in oscillation frequency f : $\Delta f/f_0 = v/v_0$. Changes in oscillation frequency of 1 Hz can be resolved with devices operating at 100 MHz; consequently, the limit of mass resolution is approximately $0.5 \text{ ng}/\text{cm}^2$.

The APM sensor was instrumented for monitoring jet fuel degradation by sealing the device into a metal flatpack (having a machined access hole) using a high temperature RTV silicone rubber sealant (see Figure 8). After soldering the flatpack into a brass test case, the test case was placed in an environmentally controlled oven and a teflon cell was compressed against the flatpack to make a liquid-tight seal. A sample (1.5 ml) of JP-8 jet fuel was added to the teflon cell and, in some cases, a small amount (0.015 ml) of ethylhexanoic acid (EHA) was added to enhance deposition. The fuel contacted the back side of the APM device. A condenser was placed in the top of the cell and a water/ethylene glycol mixture at 10°C was passed through the condenser at a rate of approximately 100 ml/min to prevent evaporation of the jet fuel. A thin teflon tube running down the condenser was used to slowly bubble oxygen into the jet fuel in the cell. The test case was connected to external electronics for operating and monitoring the APM device.

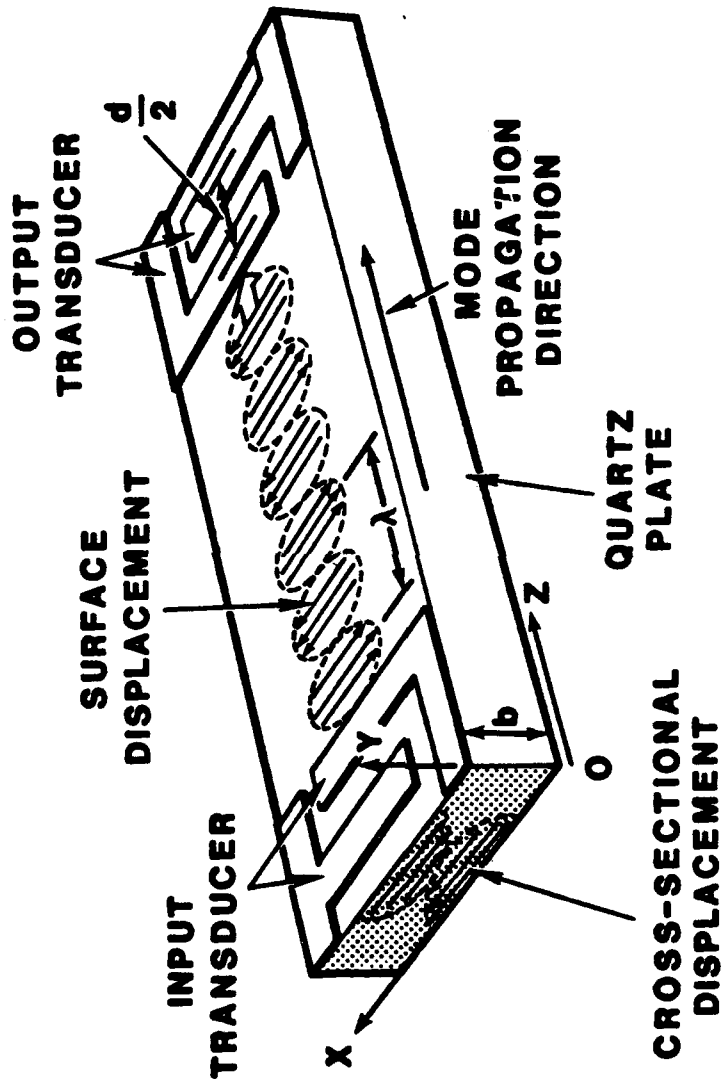


Figure 7. Schematic of an acoustic plate mode (APM) device showing the shear horizontal (SH) displacement of the mode. Each transducer consists of 75 interdigitated electrode pairs, (one is shown).

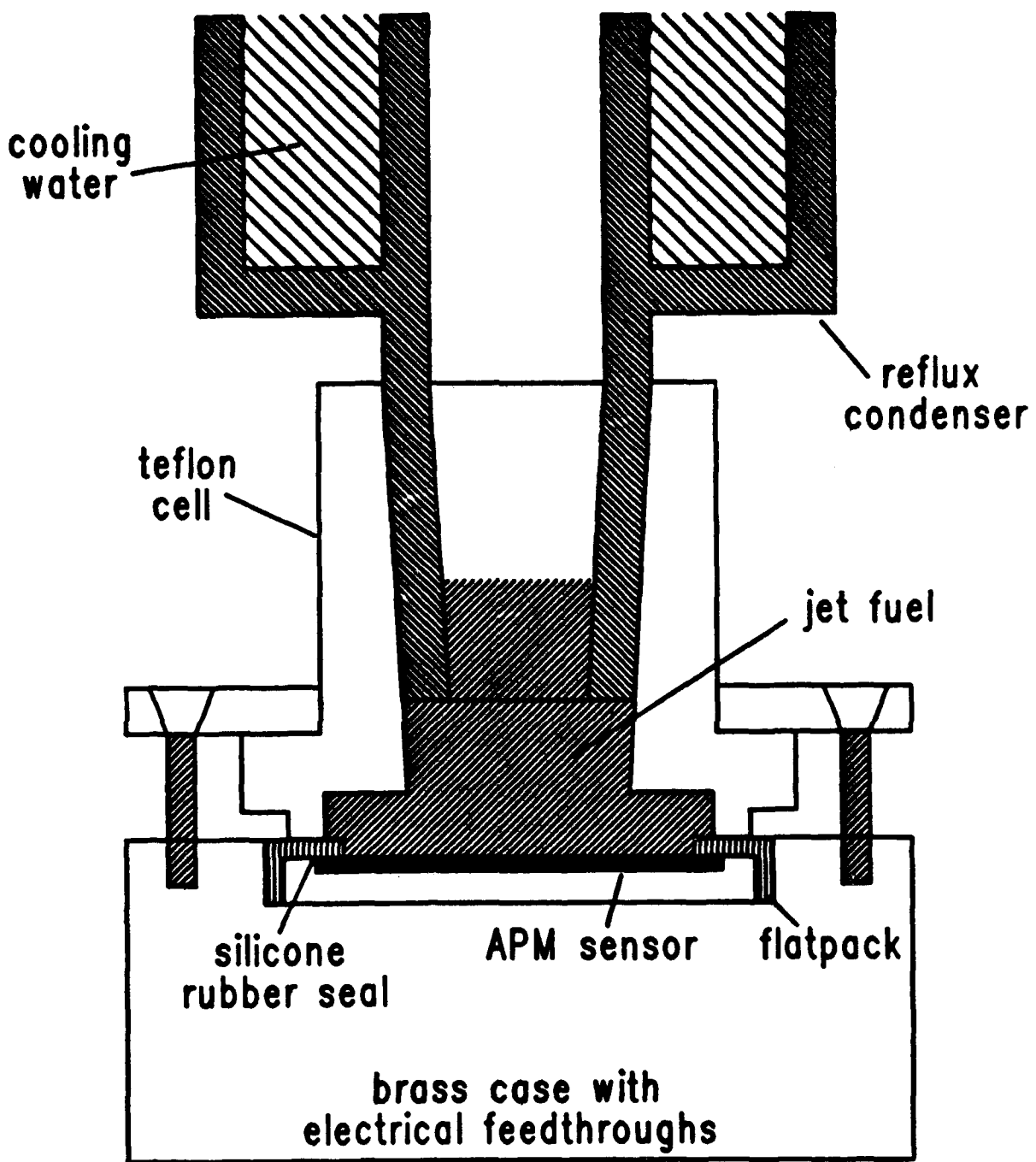


Figure 8. Cutaway view of acoustic plate mode (APM) sensor with teflon cell and reflux condenser.

While monitoring changes in both the wave velocity (as indicated by frequency) and attenuation, the oven was used to heat the device to temperatures of 150°C, 167°C and 184°C. After each run, the device test case was removed from the oven, the jet fuel was saved for later analysis and the APM device and teflon cell were cleaned using organic solvents.

Results of APM Jet Fuel Tests.

In each case, the velocity decreased significantly during the heating of the jet fuel on the device. After the temperature in the oven had stabilized, the velocity continued to decrease. In general, this decrease was approximately linear and, assuming that this response was due to a mass increase occurring during deposition of jet fuel degradation by-products, this linear rate could be used to calculate a deposition rate. For example, data for the three runs of JP-8 with EHA are shown in Figure 9 with a linear least squares fit through the data. Even though the data for each run does exhibit a significant amount of noise, a definite downward trend in the data is observed. A summary of the rates determined from this linear region of the data are given in Table 5. The mass accumulation value is calculated from Equation 7, assuming the frequency shift (Δf) is due solely to changes in surface mass density ρ_s . Rates of film deposition are calculated assuming the density of the deposited layer is 1.0 g/cm³.

Table 5. Summary of Results of APM Studies of Surface Deposition Caused by Thermal Degradation of JP-8 Jet Fuel.

Run Temperature °C	EHA added	Frequency Shift ppm/min	Mass Accumulation ng/cm ² -min	Mass Accumulation μm/day	Rate of Film Deposition mm/yr
150	N	-0.27	14	0.2	0.075
167	N	-0.4	21	0.3	0.11
184	N	-0.6	32	0.46	0.17
150	Y	-1.28	67	0.97	0.35
167	Y	-0.65	34	0.49	0.18
184	Y	-0.85	45	0.64	0.24

The results for JP-8 without the EHA show the expected trend of increased deposition rate with increasing temperature. There is significant noise in these runs, especially the 150°C run, making a quantitative interpretation of these results questionable. The EHA study shows increased deposition rate with temperature only for the two higher temperatures. In this case, the 150°C run yields the largest deposition rate of any of the experiments. The cause of this unexpected result is

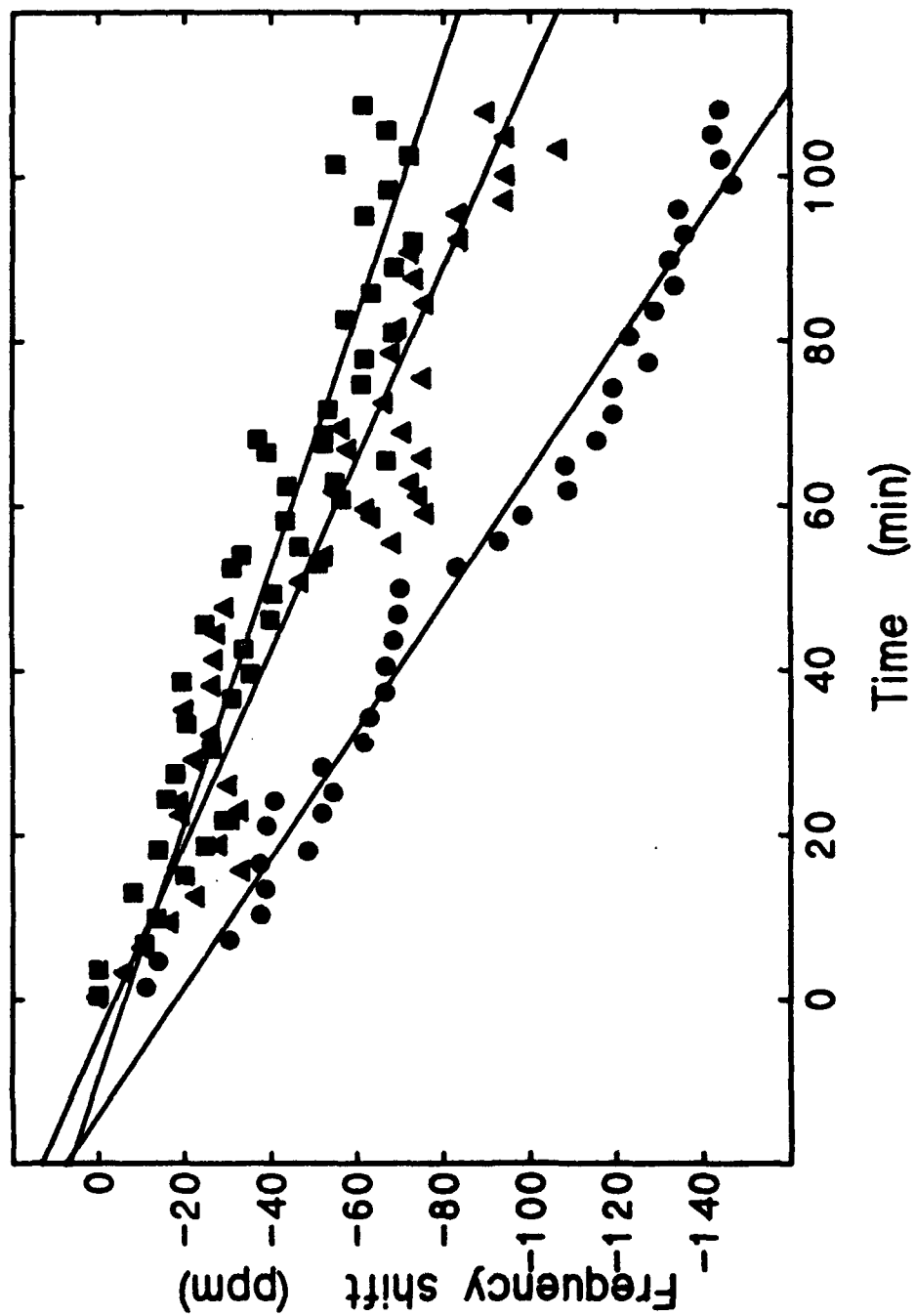


Figure 9. APM frequency response vs. time during thermal degradation of 1.5 ml JP-8 and 0.015 ml EHA under flowing oxygen. The temperature of the runs were (●) 150, (■) 167, and (▲) 184°C.

unknown. It has been observed, however, that high-temperature jet fuel causes significant swelling of the RTV silicone rubber seal around the device. We believe that stresses imposed on the device caused by swelling of the seal leads to a response unrelated to mass accumulation. The possibility that at least part of the device response observed during the runs listed in Table 5 was due to seal degradation weakens the interpretation of the results and casts doubt on the deposition rates extracted. The sealing difficulties indicate that significant improvements in the sealing technology must be achieved in order to obtain reproducible, quantitative values for deposition rates. For this reason, an alternative device that can be suspended in jet fuel and thus requires no seal to contact the device was examined. This device is the quartz crystal microbalance (QCM).

2. Quartz Crystal Microbalance (QCM) Operation

The quartz crystal microbalance (QCM) is configured with electrodes on both sides of a thin disk of AT-cut quartz (see Figure 10). The quartz crystal can be electrically excited into a thickness-shear resonance at frequencies for which the crystal thickness is an odd multiple of half the acoustic wavelength. The device can be submersed in liquids of low electrical conductivity (or contacted on a single face by liquid) to function as a solution phase microbalance. Figure 11 shows a cross-sectional view of a QCM loaded on one side by a mass layer and a contacting liquid. The change in resonant frequency Δf with surface mass density ρ_s is

$$\Delta f/f_0 = -\rho_s/(\rho h) \quad (8)$$

where f_0 is the unperturbed resonant frequency, ρ is the quartz density and h is the quartz thickness. Because the resonant frequency is simply related to mass accumulated on the crystal surface, the device can be used as an extremely sensitive microbalance and could serve as a basis for monitoring jet fuel degradation by-products accumulating on a submersed QCM. Changes in resonant frequency of 0.1 Hz can be resolved with devices operating at 5 MHz; consequently the limit of mass resolution is approximately 1 ng/cm².

QCMs operating in solution are also sensitive to the viscosity and density of the contacting solution. The extent to which jet fuel viscosity changes during degradation can also be investigated. This parameter value is required for interpretation of the PCS measurements discussed in a previous section. When the electrical characteristics are measured over a range of frequencies near resonance, we have shown that the QCM can be sufficiently well characterized to differentiate between changes in surface mass and changes in properties of the contacting liquid, in particular the liquid density-viscosity product.

The QCM electrical characteristics can be evaluated using the electrical admittance (the reciprocal of impedance), defined as the ratio of current flow to applied voltage. The electrical admittance is determined from

Quartz Crystal Microbalance (QCM)

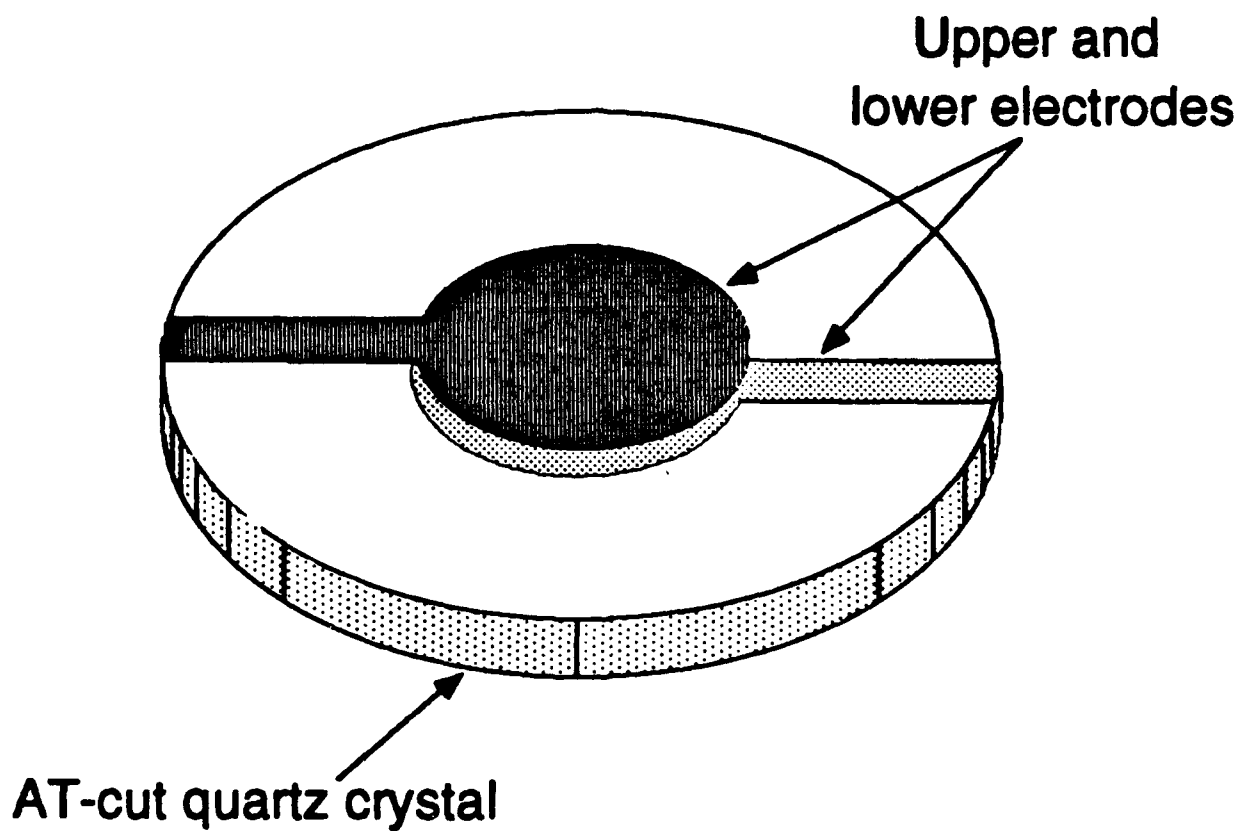


Figure 10. Schematic of quartz crystal microbalance (QCM), consisting of circular electrodes patterned on both sides of a thinned AT-cut quartz disk.

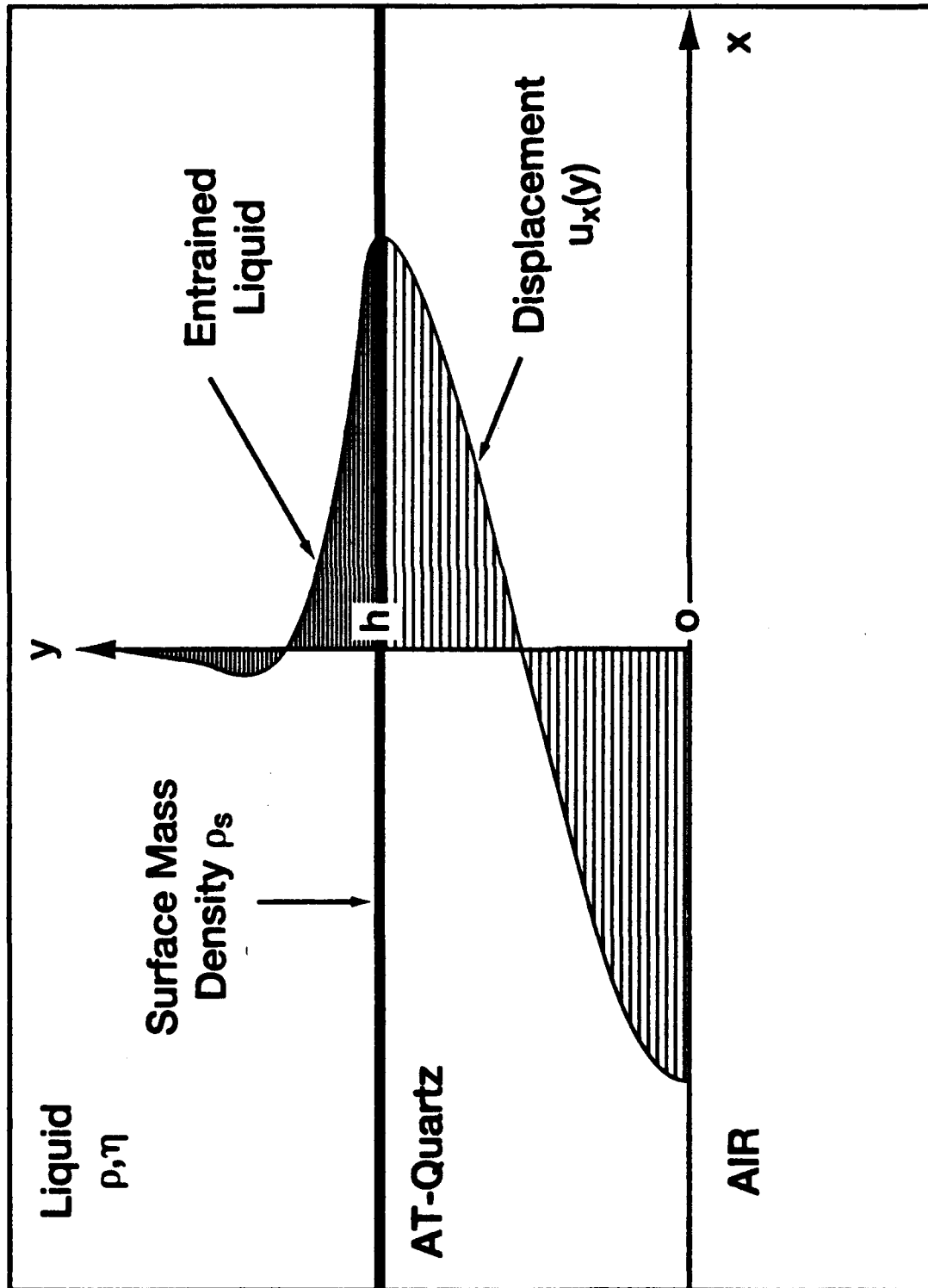


Figure 11. Cross-sectional view of a QCM simultaneously loaded on one side by a mass layer and a contacting liquid.

network analyzer measurements. An equivalent circuit model has been developed that simulates the electrical characteristics of the QCM over a range of frequencies near resonance. This model, shown in Figure 12, explicitly relates the circuit parameters to physical properties of the QCM as well as the surface mass layer and contacting liquid. Fitting the circuit model to admittance-vs.-frequency measurements thus allows extraction of surface mass and liquid properties.

Experiments were performed to characterize the effect of mass and liquid loading on the QCM response and compare with responses calculated from the model of Figure 12. Figure 13 indicates the effect on QCM admittance of changes in the properties of a liquid contacting the QCM. As the product of liquid density ρ and viscosity η increases, we note both a translation of the peak toward lower frequency as well as increased damping. Figure 14 indicates the effect on QCM admittance of a change in surface mass. As surface mass increases, we note a simple translation of the resonance peak. This translation occurs when the device is operated in air or in contact with a liquid. The qualitative difference in the admittance-vs.-frequency curves obtained with liquid or mass loading indicates the possibility of differentiating surface mass from changes in liquid properties. Measuring admittance-vs.-frequency curves at periodic intervals allows the determination of surface mass and liquid density-viscosity product as a function of time. Software has been developed that retrieves these network analyzer scans, fits the model (Figure 12) to the data and extracts surface mass and liquid density-viscosity. Initial studies on gelling solutions have indicated the ability to simultaneously monitor changes in solution viscosity and accumulated surface mass. Mass resolution is better than 1 ng/cm² for room temperature measurements.

A test fixture was designed and constructed to allow a quartz crystal microbalance to monitor jet fuel degradation at elevated temperature. This fixture, shown in Figure 15, consists of a stainless steel chamber with an O-ring seal to contain jet fuel vapors. The jet fuel is contained in a Pyrex cuvette recessed in the stainless steel housing. Pyrex was selected because this material is not expected to significantly catalyze degradation or other chemical reactions in the jet fuel. The QCM jet fuel monitor is suspended by clamps at the upper edge with the acoustically active area submersed in the jet fuel. Electrical measurements are made on the QCM through a 3.5-mm RF connector which contacts the circular electrode pattern on the QCM. Gas ports are provided on the lid of the fixture; these allow oxygen or other gases to be pumped into the fuel during the test, as well as allowing vapors to be exhausted or a N₂ purge to flow across jet fuel. A band heater is clamped around the periphery of the housing to heat the chamber. Thermocouples embedded in the base of the chamber indicate chamber temperature. A temperature controller utilizes the thermocouples to sense chamber temperature and controls current flow to the band heater to maintain a preset temperature. Using this controller, chamber temperature has been regulated up to temperatures near 250°C, with no degradation of the QCM sensor. This is a significant improvement in operability compared with the acoustic plate mode sensor system.

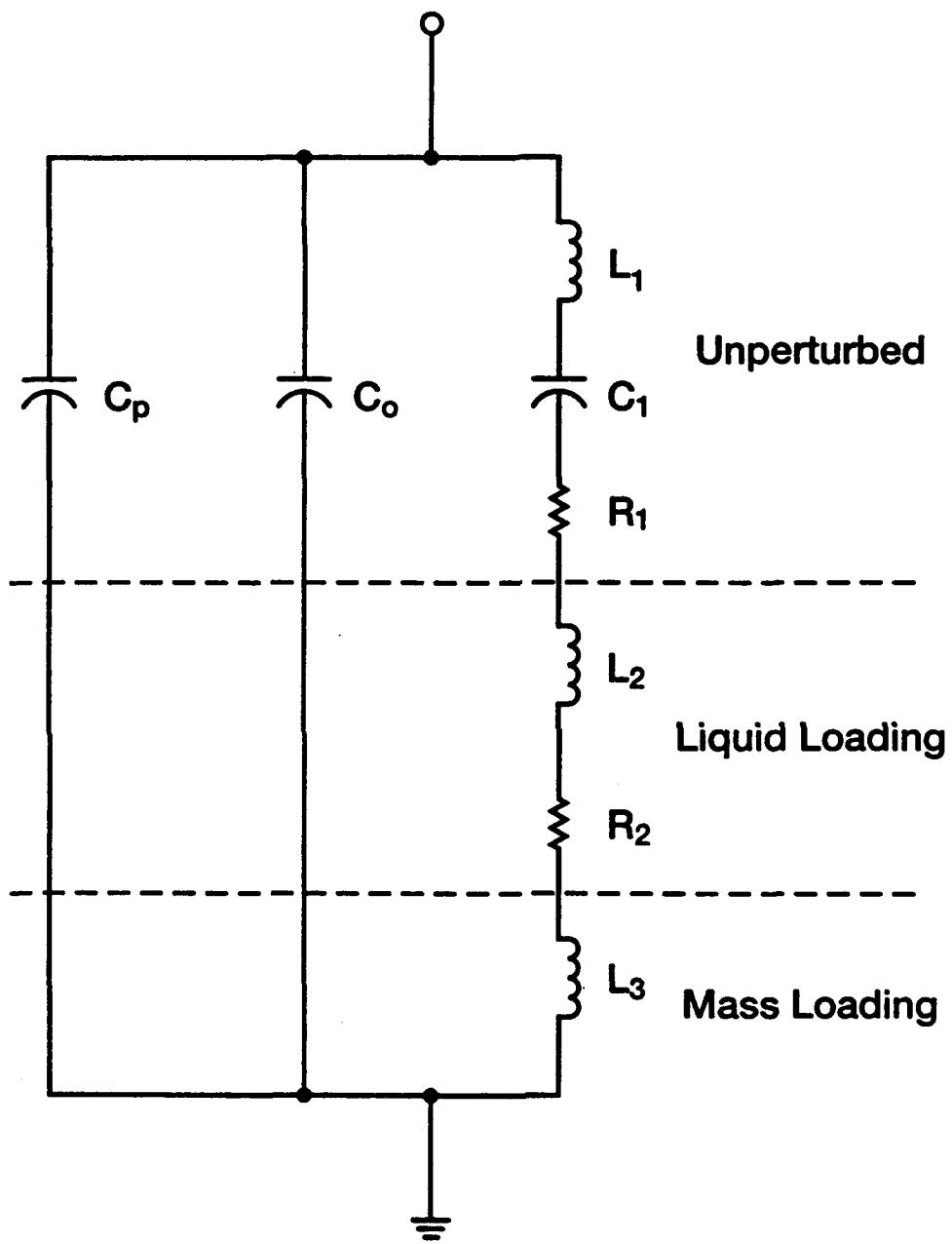


Figure 12. The equivalent circuit for a QCM under mass and liquid loading including parasitic capacitance in the test fixture C_p .

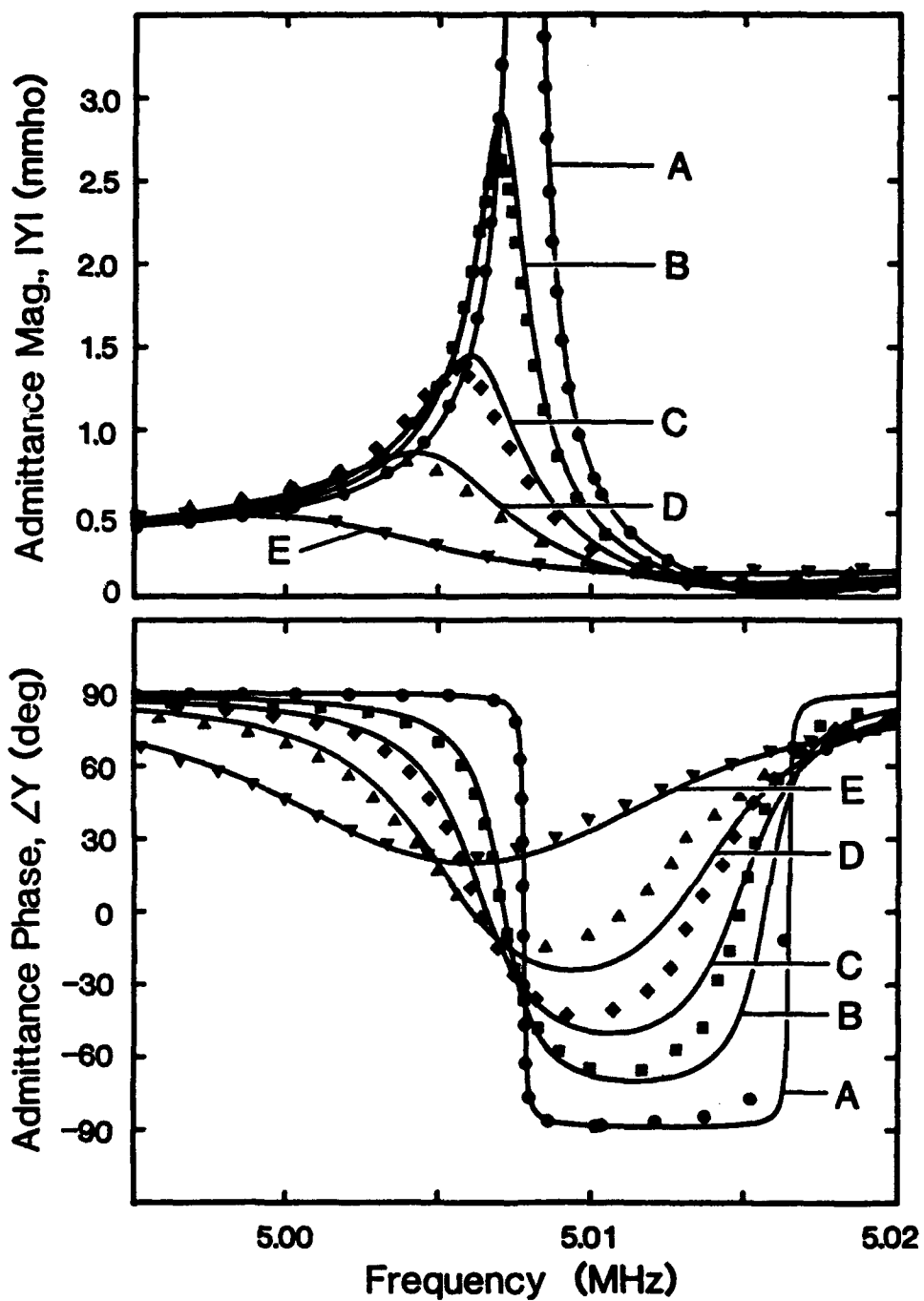


Figure 13. QCM admittance measured (points) and calculated (lines) near the fundamental resonance as the density-viscosity product ($\rho\eta$, $\text{g}^2/\text{cm}^4\text{-s}$) of a contacting fluid increases: (A) air, $\rho\eta = 2 \times 10^{-7}$; (B) water, $\rho\eta = 0.010$; (C) 43% glycerol in H_2O , $\rho\eta = 0.044$; (D) 64% glycerol in H_2O , $\rho\eta = 0.15$; (E) 80% glycerol in H_2O , $\rho\eta = 0.72$.

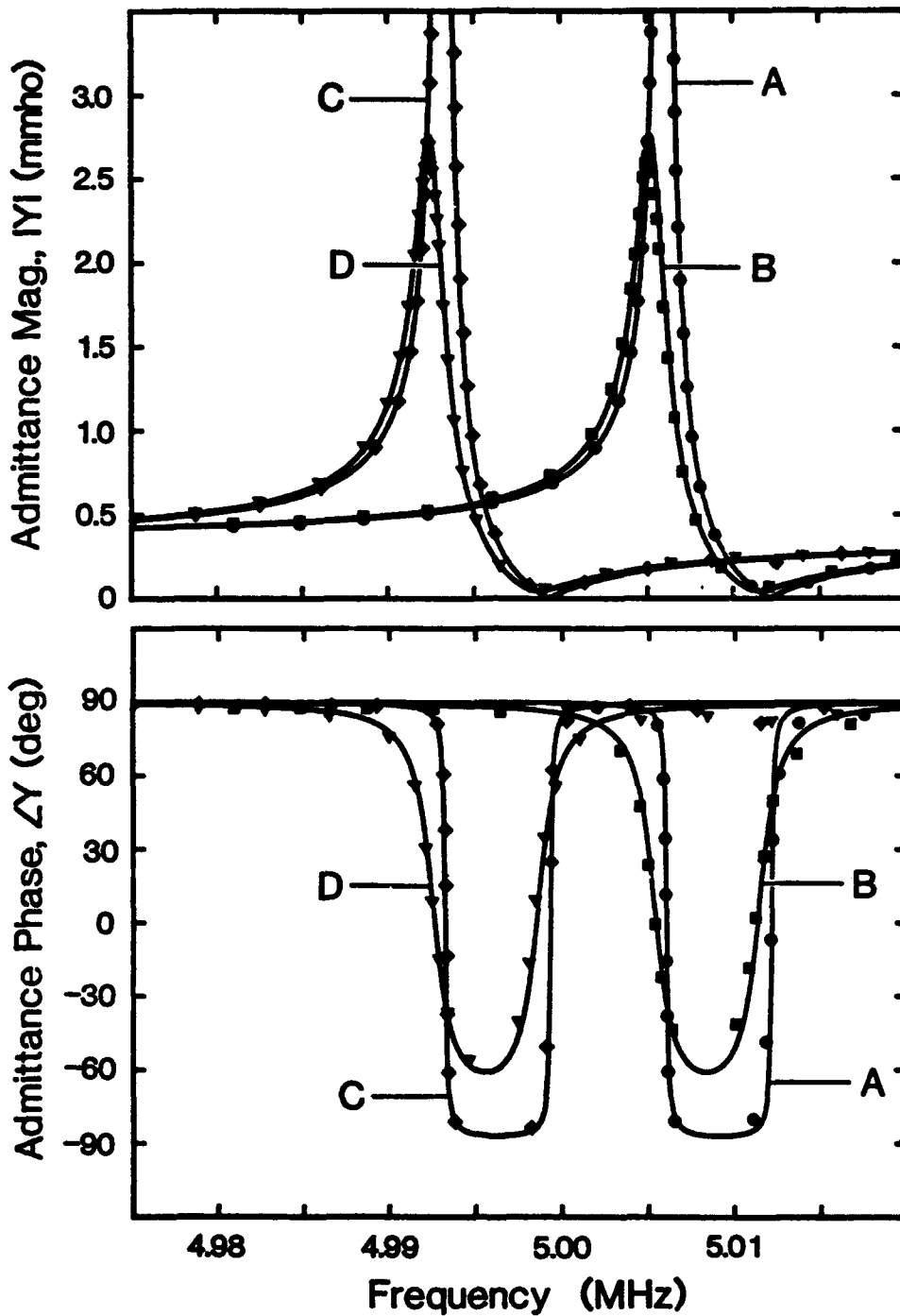


Figure 14. QCM admittances measured (points) and calculated (lines) before and after deposition of a 124 nm Au layer. Before Au deposition: (A) in air, (B) in water; after Au deposition: (C) in air, (D) in water.

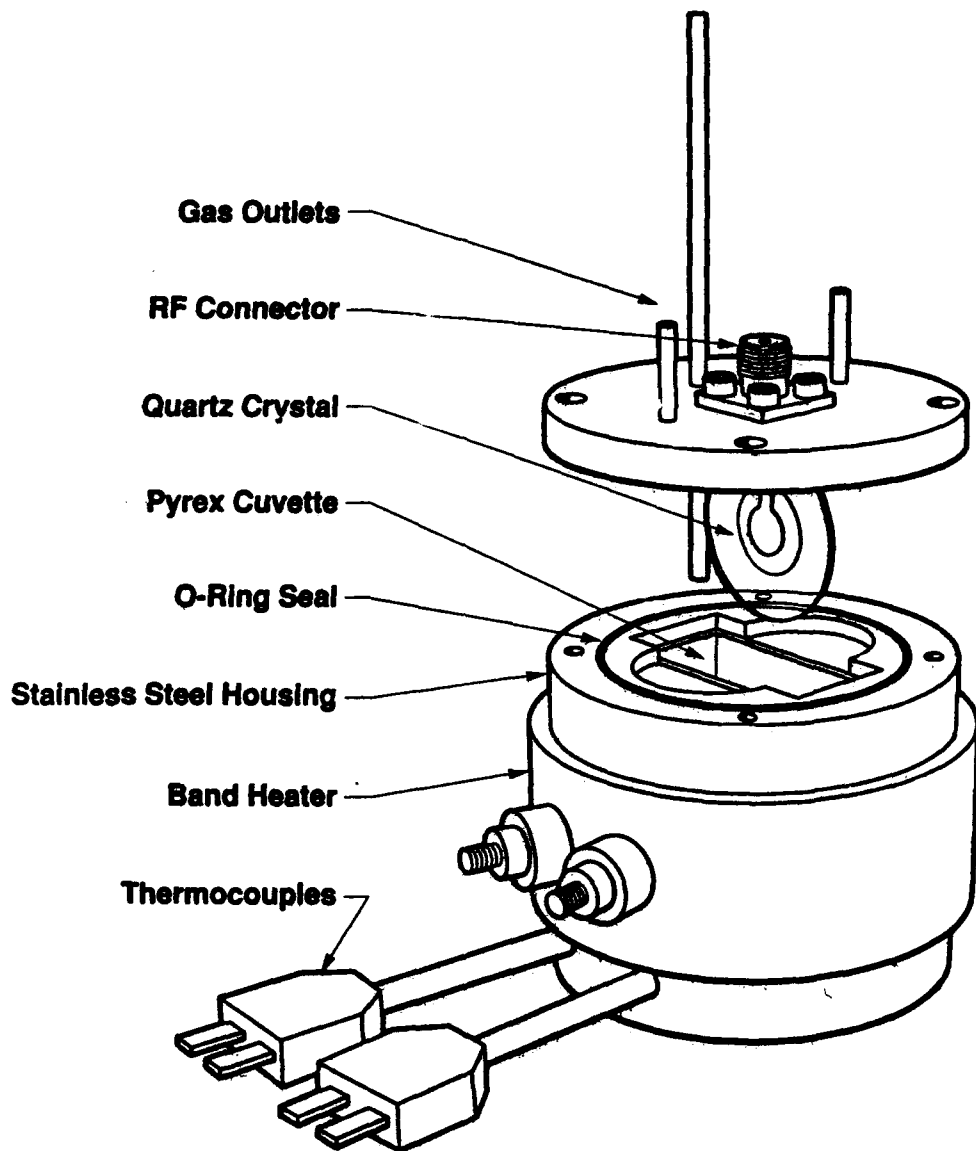


Figure 15. Test fixture that uses a QCM to monitor jet fuel properties at elevated temperatures. A temperature controller uses thermocouples to measure chamber temperature and regulates power to the band heater to maintain a preset temperature.

To measure the frequency-dependent electrical characteristics of the QCMs, a network analyzer was connected to the RF connector of the test fixture. Swept-frequency measurements of reflection are made, from which electrical admittance is determined. To date, measurements of QCM admittance-vs.-frequency have been performed up to 200°C in air and 40°C in unstressed jet fuel. The ability to make measurements on the QCM at elevated temperatures, with temperature held constant to 0.1°C over 24 hours has been demonstrated. Figure 16 shows the admittance characteristics for a QCM in air and suspended in jet fuel. By fitting the data to the model of Figure 12, the surface mass accumulation (<1 ng/cm²) and density-viscosity product (0.015 g²/cm⁴-s) were obtained at room temperature. At 40°C, the density-viscosity product extracted was 0.0084 g²/cm⁴-s, comparable to the literature value [10] for a "typical" jet fuel of 0.0075. Current and future testing will focus on evaluating the kinetics of fuel degradation at elevated temperatures and metal-fuel interactions.

C. LIQUID AND SOLID CHARACTERIZATION STUDIES

Thermal stress studies were performed on JP-8 and Jet A-1 fuels to investigate solubility effects of formed solids at elevated temperatures and to determine the effect on subsequent FTIR spectra of supplying oxygen to the fuel during heating. Studies were also performed on an aircraft afterburner injector arm obtained from Wright-Patterson AFB. This component contained deposits from fuel degradation. The studies were performed to determine elements present in the deposit and the afterburner injector arm and to estimate the temperatures at which the deposits were formed. These studies are described in the succeeding sections.

1. Thermal Stress Tests on JP-8 Fuel

A series of thermal stress tests on JP-8 jet fuel were run to determine solubility effects on formed solids. Table 6 presents the matrix of tests performed and observations on the results. Initially, eight tests were performed at increasing temperatures to determine a baseline response as a function of temperature, followed by performing five tests to look at the solubility aspects of the formed solids. Each run was performed by first taking JP-8 and preparing it by bubbling oxygen through it for about 15 minutes. Approximately 15 ml of the fuel was put in a stainless steel bomb overpressured with air to 300 psig and placed in a sand bath. The bath and fuel was heated to constant temperatures of 160, 181, 200, 225, 250, 299, 350, and 399°C for 1 hour. The heat-up period ranged from 2 to 3 minutes and the cool-down period ranged from 1 to 2 minutes. Table 7 presents analyses of the gas products from each of the runs.

Consistent with previous experiments, the amount of sediment and darkening of the stressed fuel increased with temperature from the 160°C to the 225°C run (dark brown in color). The 250°C run had slightly less sediment and was less dark. The 300°C run had no visible sediment particles and was a yellow-orange color. The 350°C and 400°C runs darkened in color

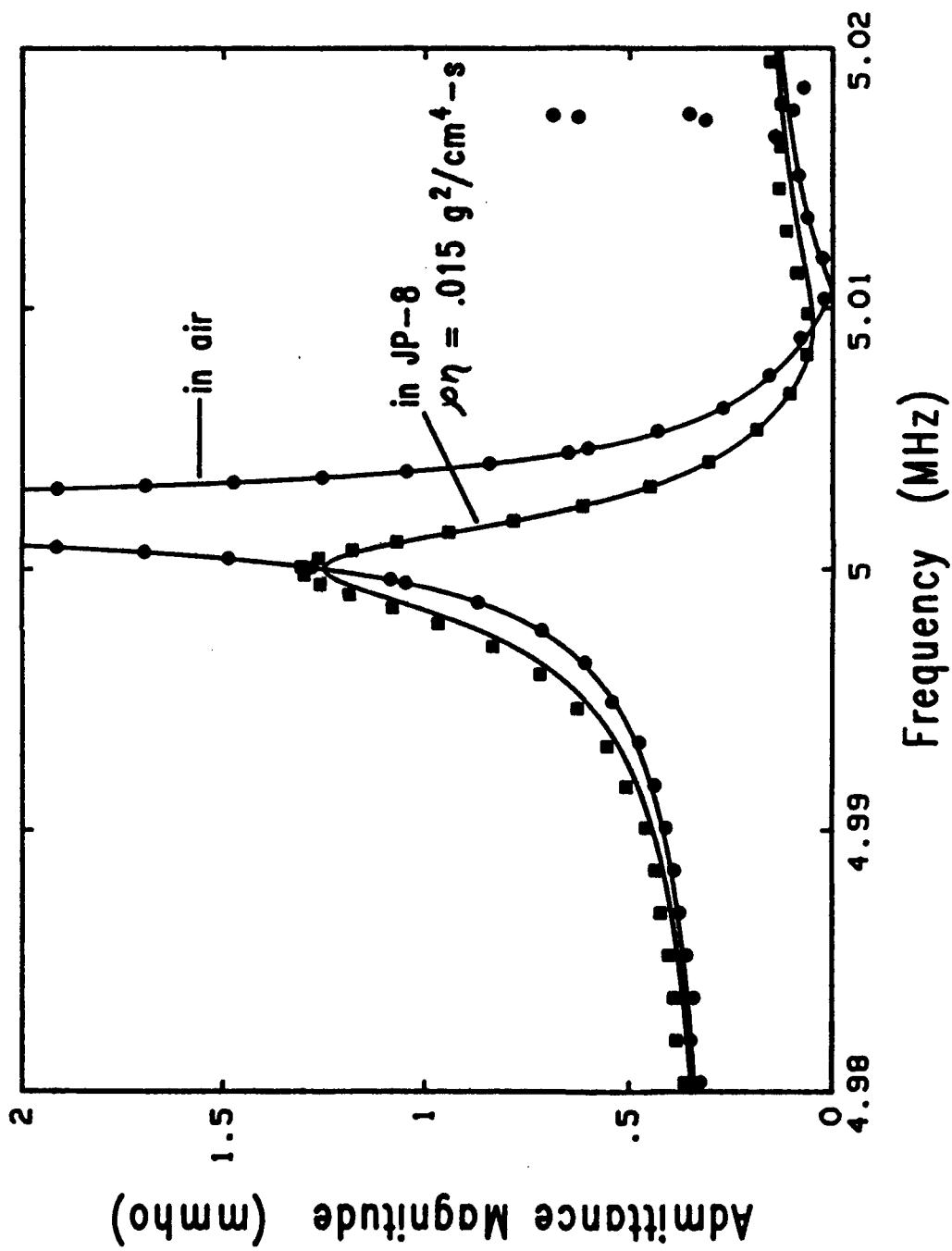


Figure 16. QCM admittance measured (points) and calculated (lines) before and after immersion in JP-8 jet fuel at 20°C. The viscosity-density product calculated from the curve for the jet fuel is indicated.

Table 6. JP-8 Thermal Stress Test Matrix and Observations

TEMPERATURE, °C	OBSERVATIONS
No stressing	Although the JP-8 fuel sample received from Wright-Patterson was clear, the fuel has degraded somewhat and is a very light straw color. PCS shows no significant particles however in the unstressed fuel.
160	This sample is slightly darker than the unstressed fuel with no visible sediment.
181	This is again slightly darker, turning yellow-orange with again no visible sediment.
200	This sample turned a light brown with sediment becoming visible.
225	This sample turned a dark brown with a substantial amount of sediment. When the sediment was removed, the liquid was an orange-brown color.
250	This sample was dark brown with a substantial amount of sediment, although visually less than the previous sample.
299	This sample was an orange-yellow, closest in color to the 181°C sample with no visible sediment.
350	This sample was slightly darker than the previous sample but again contained no visible sediment.
399	This sample was again slightly darker and perhaps contained a small amount of suspended solids.
300; hexadecane	No visible change occurred except for a slight color darkening that might have been because of impurities in the tubing bomb system.
300; C ₁₆ + solids	The stressed liquid and solids turned brown and the solids did not appear to re-solubilize significantly.
300; C ₁₆ + liquid from 225°C.	No significant change.
250°C, cool a few days, then 300°C.	No significant change.
225°C, cool 1 hr, the 300°C.	No significant change from heating only to 225°C.

Table 7. Gas Analyses on Jet Fuel JP-8 Tubing Bomb Thermal Stress Tests
(All tests performed for 1 hr under 300 psi air)

TEMP (°C)	Compositions of Specified Gas Components								
	O ₂ /N ₂	N ₂	O ₂	CO	CO ₂	CH ₄	C ₂ H ₄	C ₂ H ₆	TOTAL
160	0.24	77.84	18.89		0.08				96.81
181	0.26	78.75	20.22	0.02	0.003				96.63
200	0.23	80.33	18.24	0.14	0.1				98.99
225	0.20	82.08	16.69	0.30	0.17	0.02	0.04	0.003	94.56
250	0.21	81.33	16.94	0.38	0.17	0.15		0.06	99.09
299	0.20	80.55	16.00	1.08	1.29	0.12	0.04	0.008	99.03
350	0.09	80.03	7.18	4.53	3.72	0.89	0.21	0.072	98.82
399	0.13	80.00	10.78	0.36	0.97	1.65	0.23	0.57	99.30

compared with the 300°C run. The oxygen fraction appeared to decrease slightly through the 300°C test, with a dramatic decrease during the 350°C and 399°C tests. Carbon monoxide and carbon dioxide began to appear early, with the fractions increasing with temperature until the 399°C test. Measurable quantities of methane, ethane, and ethene began to appear during the 225°C test, with the fractions increasing at higher temperatures.

Five additional tests were performed to examine the solubility of solids formed from the jet fuel stressing. The separated liquids and solids from the 225°C test were each added to hexadecane and heated to 300°C, along with a run heating hexadecane alone to 300°C. In the fourth test, the solids and liquids from the 250°C test were heated to 300°C. In the fifth test, we heated JP-8 to 225°C for 1 hr under 300 psig air as before, cooled the samples for 1-2 hours and then heated it to 300°C. The hexadecane control sample did not form sediment or change color significantly.

In the test with the solids added to the hexadecane, a substantial amount of the solids still remained after stressing at 300°C (because of the small amount of solids and the difficulty in quantitatively separating and measuring them, we could not compare the amount of solids before and after the test). A small amount of sediment was apparent in the sample of hexadecane plus stressed jet fuel, but may have been residual sediment that we were not able to remove from the liquid. The 250°C sample still looked approximately the same after re-stressing at 300°C. The sample stressed to 225°C, cooled, and re-stressed at 300°C had a significant amount of solids and did not look visually different than the sample stressed only at 225°C. In summary, the solids did not appear to significantly re-solubilize at 300°C although, if the fuel is stressed at 300°C without spending a significant amount of time at a lower temperature, little to no sediment is formed.

2. FTIR Analyses

FTIR analyses were performed on JP-8 fuel samples before and after thermal degradation had occurred. Only very small differences in spectra were measurable when the samples had been stressed in microautoclave reactors with an overpressure of air or inert gases. Modifications made to the FTIR cell configuration to increase the cell path length enhanced the differences in the spectra a small amount, but the amount of difference in oxygenated functional group peaks was still only on the order of tens of milliabsorbance units. Samples were then tested by FTIR that included the unstressed sample, samples saturated with gaseous oxygen and then stressed at 180°C, and samples stressed at 180°C while bubbling oxygen through the sample. The JP-8 sample that had been saturated with oxygen prior to thermal stressing still showed only slight changes in the concentration of oxygenated functional groups (a Jet A-1 that supposedly did not contain antioxidants showed larger changes). However, a fuel sample that was thermally stressed while bubbling oxygen through the fuel showed very large changes in the same functional groups as compared with the pre-saturated sample. Obviously, the availability of oxygen makes a significant difference. Because the condition of constant availability of oxygen is not a realistic operating condition, FTIR is expected to be used on a limited basis to determine changes in the concentrations of oxygenated functional groups. The technique is still expected to be of use on a general basis to investigate the composition of the jet fuel liquids and formed solids.

3. Analyses of Afterburner Injector Arm and Deposits

Part of an aircraft component, an afterburner injector arm, containing deposits formed during aircraft operation was received from WPAFB for analysis. The component contained deposits with two visually distinct morphologies. One was a porous, granular deposit that occurred in relatively large quantities and thicknesses and the other occurring in thin flakes with a silver-gray luster, suggestive of a graphitic structure. It is known from the operating conditions in the afterburner section that the latter deposits were formed at higher temperatures than the former. There appeared to be a distinct location in the component, approximately halfway down the arm, where the deposits switched from the porous deposits to the flakes. We noted that the regions of highest deposits were those where a disparity existed (e.g., near a hole) or a region where a thermal sink or transition existed. Additionally, a large number of spots of corrosion were present in the central hub.

Analyses of the component and the deposits include carbon-hydrogen-nitrogen analyses, Auger spectroscopy, secondary ion mass spectroscopy (SIMS), and Raman spectroscopy. C-H-N analyses were performed on deposits taken from various locations in the component. Porous deposits found contained a high carbon content, with significant amounts of hydrogen and nitrogen. The flake deposits were essentially totally carbon, suggesting a graphitic structure, with little hydrogen or nitrogen. Typical compositions for the two deposit types are shown in Table 8.

Table 8. Typical Carbon-Hydrogen-Nitrogen Compositions of Deposits from Afterburner Injector Arm

<u>Element</u>	<u>Porous Deposit (wt%)</u>	<u>Flake Deposit (wt %)</u>
Carbon	85.1%	99.3%
Hydrogen	3.9%	<0.1%
Nitrogen	0.5%	0.2%

The corrosion spots on the central hub were analyzed with Raman, Auger electron spectroscopy, and secondary ion mass spectroscopy (SIMS). Raman spectrum from the corrosion were not obtained because of the low power necessary to prevent the corrosion product from being blown away. The Auger and SIMS data indicated that the particles were predominantly carbon and oxidized titanium. The brightly colored areas around the particles contain S, Cl, C, oxidized titanium, Cu, and Zn. At this time, we do not know whether the process used in cutting the component affected the analyses of the elements detected.

A second type of material, analyzed with Auger and SIMS, are bright spots that show up optically. These features appear to be regions where the black material flaked off, exposing the underlying metal. This observation was confirmed by the surface analysis. A significant amount of electrical charging in the black area is observed, indicating a thick non-conducting region. The SIMS data from the bright areas suggests that the major constituents of this base material are Cr, Mn, and Co.

Raman spectroscopy was also utilized for solid analysis, primarily to determine if maximum temperatures as a function of position can be determined. One half of an injector tube was split lengthwise and designated sample #4 and a black chunk removed from the interior of the injector tube. We obtained spectra of these samples by Raman spectroscopy. Raman spectra were obtained by illuminating the samples with a green (514.5-nm) laser beam focused to an approximately 1.5- x 0.1-mm line. The light reflecting off the sample was analyzed for inelastically scattered components. The difference in frequency between an inelastically scattered component and the laser frequency is known as its Raman shift. When spectra are plotted in terms of Raman shifts (frequency units of cm^{-1}), peaks in intensity (or counts) represent characteristic vibrational frequencies of the atoms in the materials being analyzed. Broad fluorescence bands often underly the Raman bands in the original data from which the Raman spectra were plotted. Fluorescence results from absorption/emission of laser photons and involves electronic, rather than vibrational, energy levels. In these samples, the fluorescence is most likely due to incompletely carbonized jet fuel residues. Except as noted, the spectra included in this report have had background fluorescence removed by a fitting procedure.

We measured distances along the split injector tube in centimeters from

the "dark" end, which we assume to be the open, or outlet end. Figures 17 through 21 display Raman spectra obtained at the dark end and at distances to 13.2 cm from the dark end. Figure 17 shows spectra at the dark end and up to 2 cm from it. Two Raman bands are present in the spectrum obtained at the dark end. We believe that these Raman bands are due to metal oxides on the surface of the tube. The 553 cm^{-1} band matches well the most intense band of Cr_2O_3 , but it may include some contributions from Ni-O bonds. The 687 cm^{-1} band is probably due to spinel structures of the $\text{M}_y\text{Cr}_x\text{O}_4$ or $\text{M}_y\text{Cr}_x\text{O}_3$ type. At 10.5 cm from the dark end, the spectrum (Figure 18) includes also a band at 889 cm^{-1} , possibly because of chromate (CrO_4^{2-}) species. A black chunk was removed from the injector tube at this location, apparently baring the oxidized metal surface underneath it.

Figure 17 shows that the metal oxide Raman bands are replaced by broad bands near 1354 cm^{-1} and 1597 cm^{-1} as the spectra are obtained farther from the dark end. These bands are due to glassy carbon and are carbonized residues of the jet fuel. Glassy carbon is similar to charcoal. The peak position, bandwidth, and relative intensity of the Raman bands of glassy carbon are sensitive to temperature treatment and are indicative of the maximum temperature experienced by the carbon. At the $\sim 600^\circ\text{C}$ temperature believed to be present at the outlet of the injector tube, glassy carbon readily oxidizes to volatile species if sufficient oxygen is present. As shown in Figure 17, glassy carbon is missing at 0 cm from the dark end of the injector tube. Farther up the tube, glassy carbon was able to accumulate. The opacity of a glassy carbon deposit at visible wavelengths prevents the laser beam from sampling any underlying materials, e.g. metal oxides. The pattern of deposition of the glassy carbon may be related to temperature variation and/or the availability of oxygen.

As shown in Figure 19, glassy carbon dominates the Raman spectra from 2 cm to 13.2 cm from the dark end of the tube. Except for the spectrum obtained at 13.2 cm, the Raman bands of the glassy carbon are similar in peak position, bandwidth, and relative intensity, suggesting a flat temperature profile. The different relative intensity of the glassy carbon Raman bands at 13.2 cm indicates a different, possibly lower temperature.

Between the regions at 11.5 cm and 13.2 cm is a region containing glassy carbon that is characterized by very broad, diffuse, Raman bands (Figure 20). These diffuse bands indicate a much lower formation temperature for the glassy carbon present at 12 cm from the dark end than for the glassy carbon on either side of it. It is possible that the low temperature glassy carbon at 12 cm was formed by residual fuel during cool-down of the injector tube, while the higher temperature glassy carbon deposits on either side were formed while the injector tube was at operating temperature. In Figure 21 are plotted the original data (without removal of the fluorescence background) corresponding to two of the spectra from Figure 20. The fluorescence background increases sharply from 11.5 cm to 13.2 cm from the dark end. The increase in the fluorescence background is believed to be due to increasing amounts of incompletely carbonized,

Interior of Split Injector Tube - Sample #4

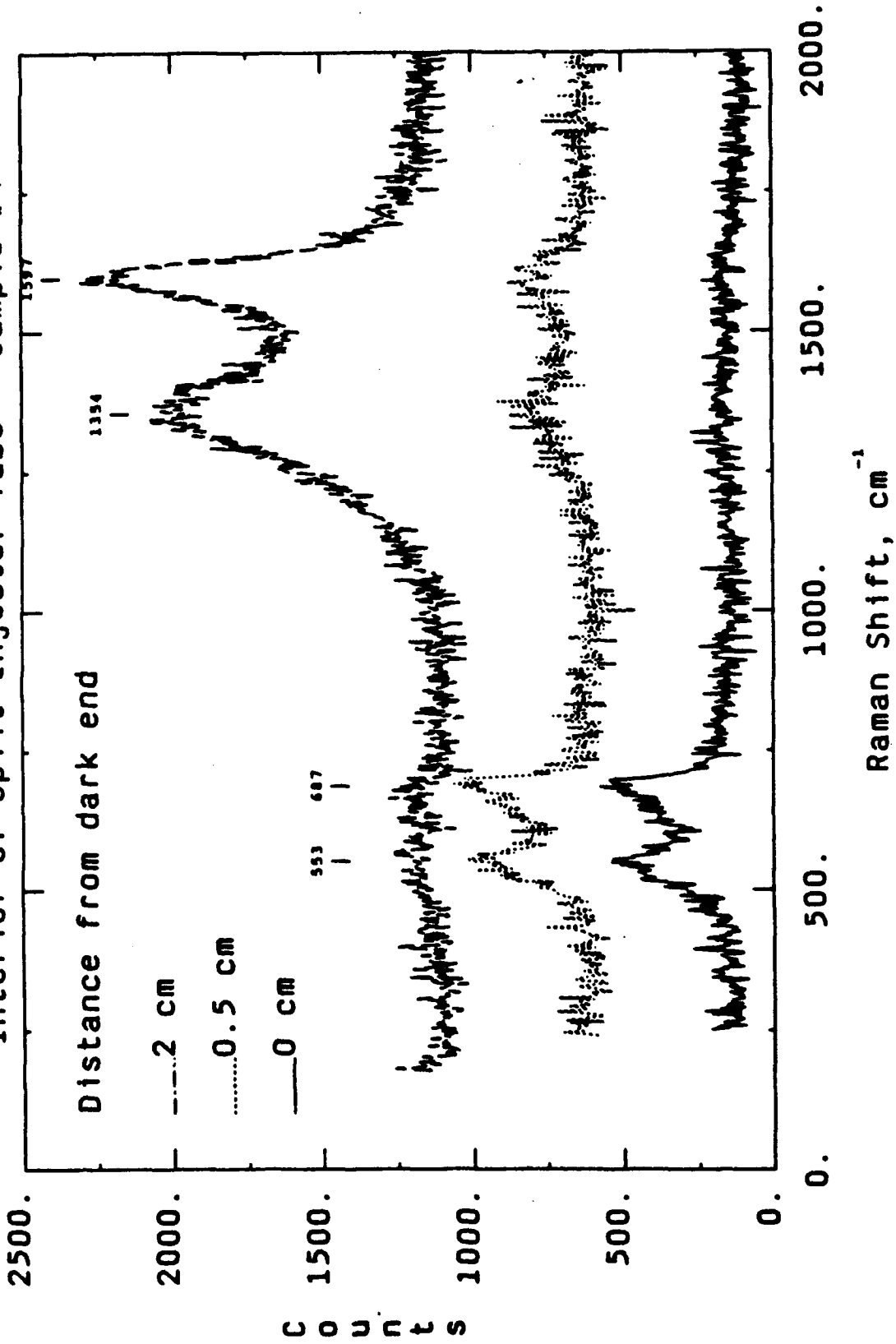


Figure 17. Raman spectra of injector arm: 0.0, 0.5, and 2 cm from tube end.

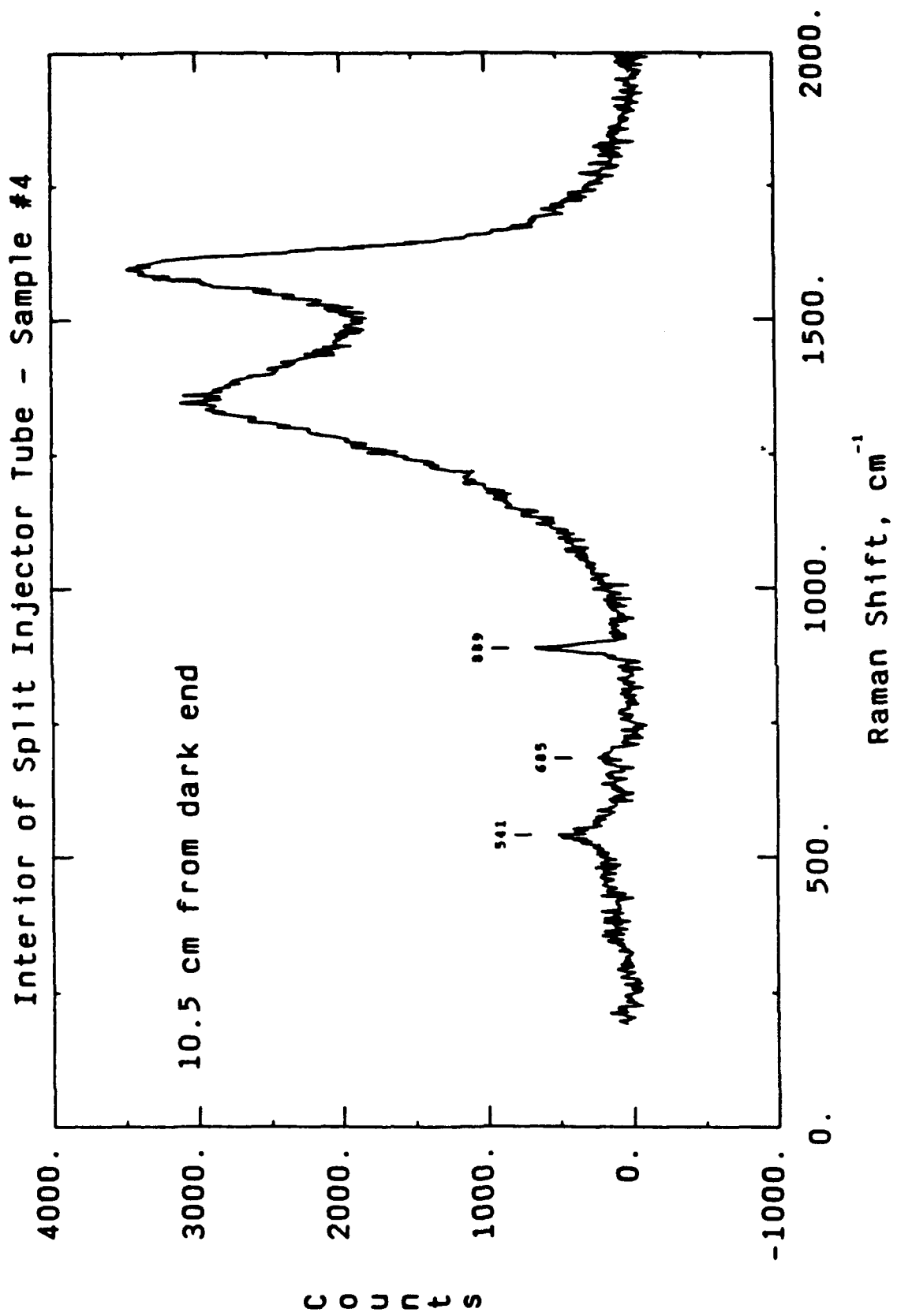


Figure 18. Raman spectra of injector arm: 10.5 cm from tube end.

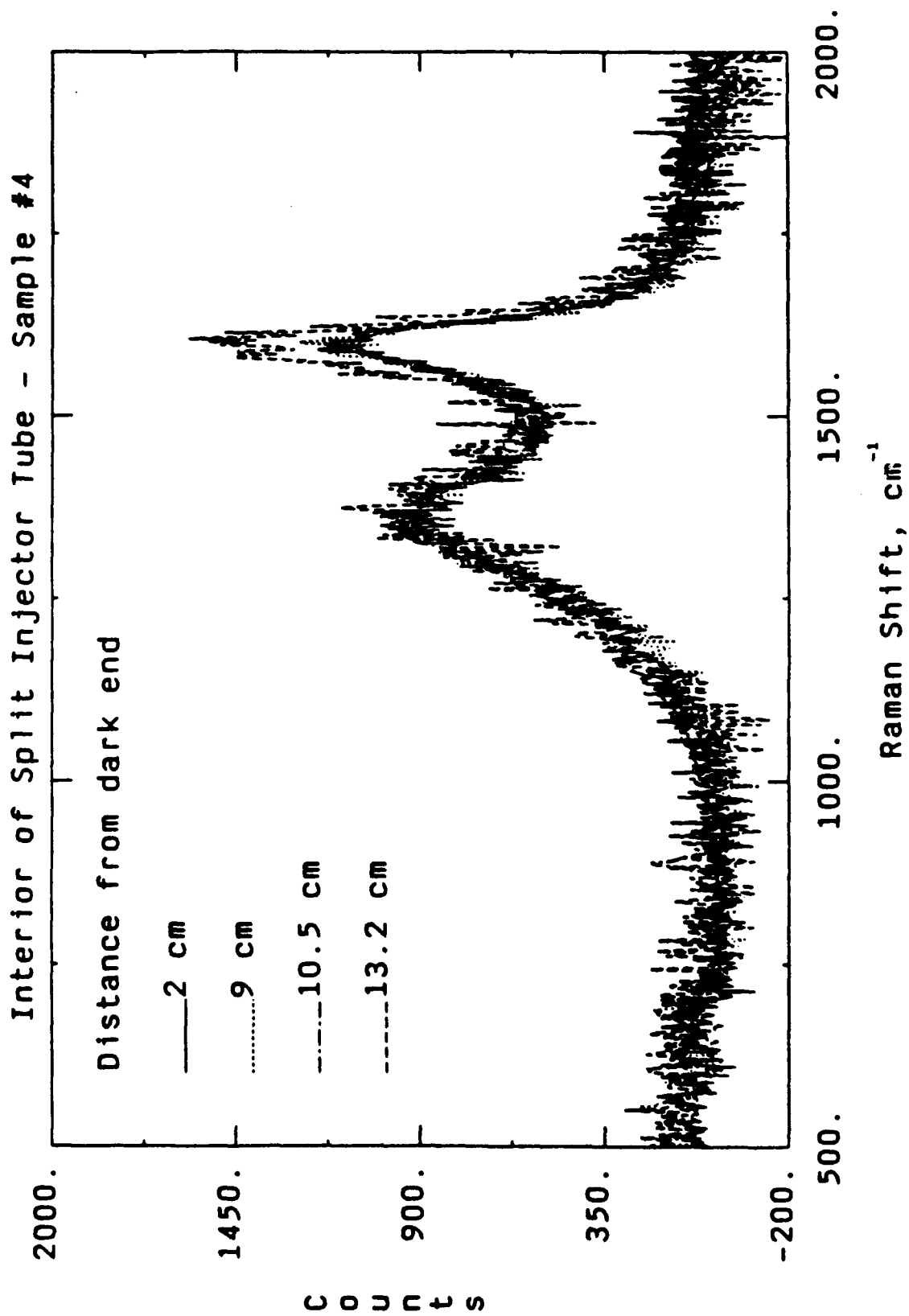


Figure 19. Raman spectra of injector arm: 2.0, 9.0, 10.5, and 13.2 cm from tube end.

Interior of Split Injector Tube - Sample #4

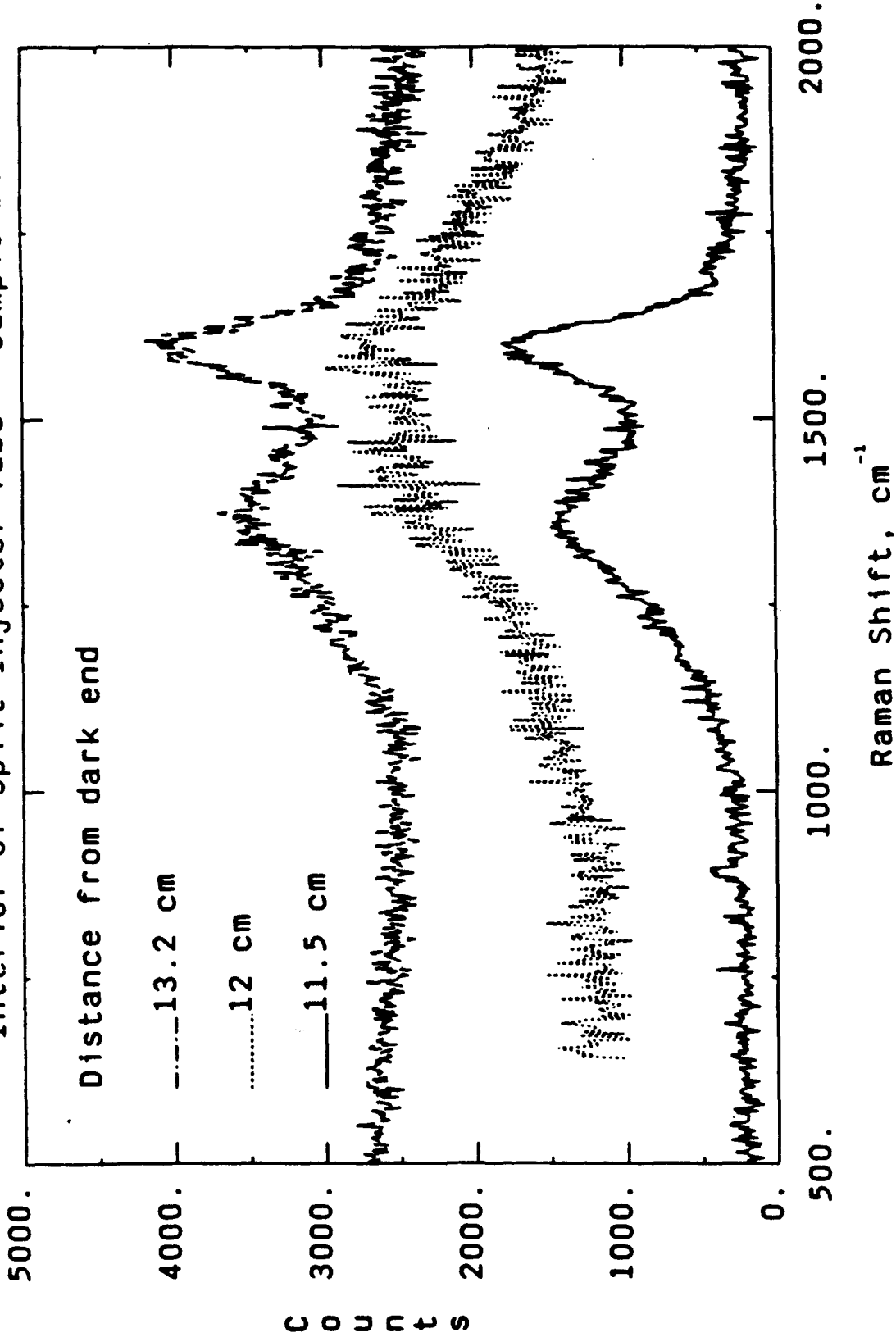


Figure 20. Raman spectra of injector arm: 11.5, 12.0 and 13.2 cm from tube end.

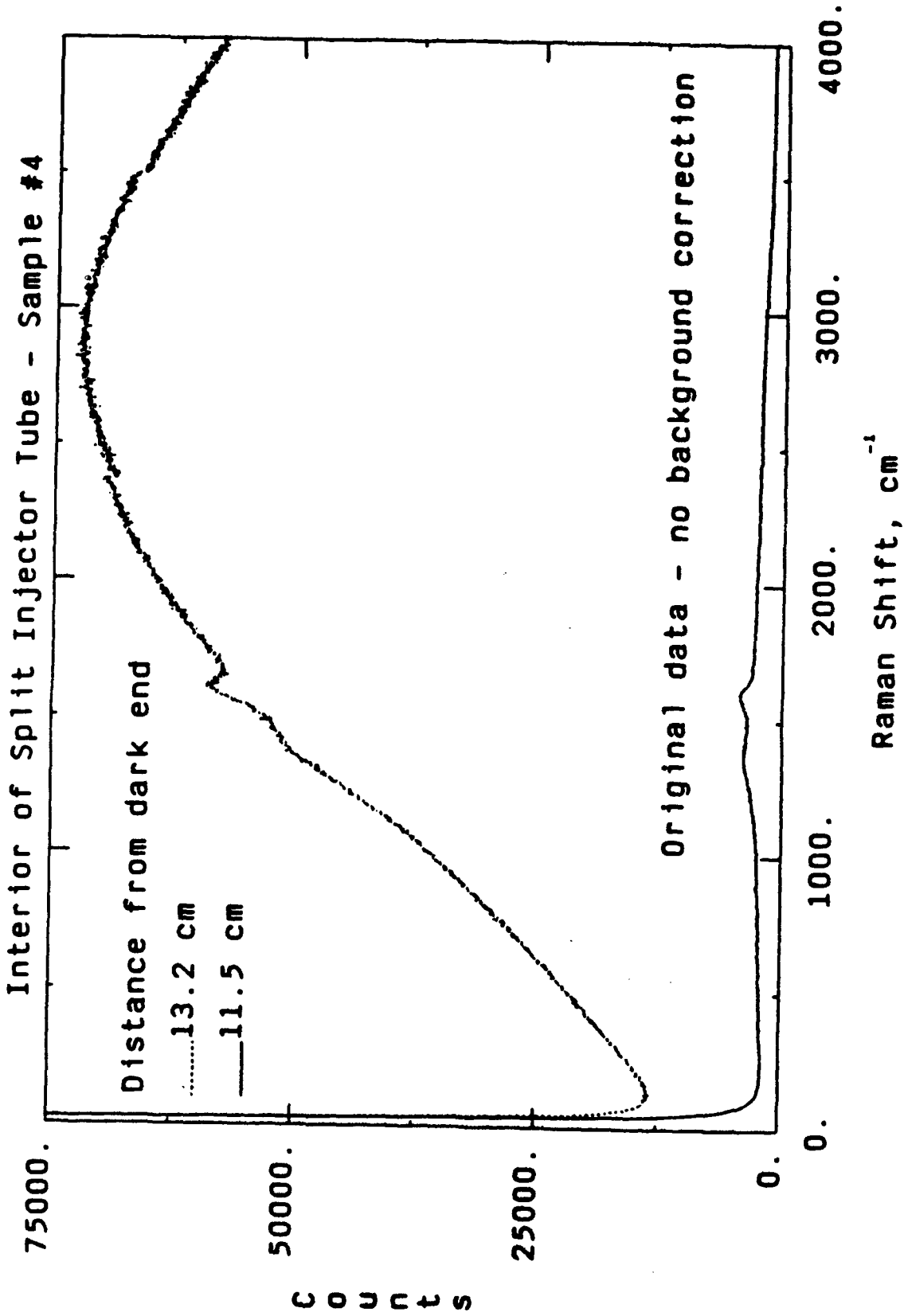


Figure 21. Raman spectra of injector arm: 11.5 and 13.2 cm from tube end; no background correction.

residual jet fuel. The black chunk found near this area may have formed from residual fuel left in the injector tube during cool-down. X-ray diffraction of the black chunk indicates that it is amorphous. The black chunk and the glassy carbon deposit at 13.2 cm from the dark end of the injector tube have nearly identical Raman spectra (Figure 22), indicating similar temperature exposures.

We are attempting to determine the temperature exposures of the glassy carbon deposits by comparing their Raman spectra to those of temperature standards, i.e. jet fuel samples carbonized at known temperatures and pressures. Only two temperature standards are currently available. They were carbonized at 550°C in 100 psi and 800 psi air (Figure 23). The black chunk has a Raman spectrum (Figure 24) that is similar, but not identical, to the 550°C temperature standards. A more extensive set of temperature standards (currently being developed) is required to assign absolute exposure temperatures to the glassy carbon deposits.

Raman analysis of glassy carbon on sample #4 indicates that a relatively flat temperature profile existed over much of its length during operation. However, the presence of lower temperature forms of carbon interspersed with higher temperature forms and variations in the level of background fluorescence because of incompletely carbonized jet fuel suggest that a temperature gradient existed during cool-down. The presence of a thick carbon deposit in the injector tube may be related to carbonization of residual jet fuel at a specific point along this temperature gradient. Additional characterization studies performed on deposits from a similar afterburner injector arm are described in Reference 11.

III. CONCLUSIONS

Development of instrumentation systems to measure quantitatively changes in physical and chemical characteristics of hydrocarbon liquids and solids was performed and initial testing completed during this year within the Advanced Thermally Stable Jet Fuels Development Program. Two important systems to measure particle size distributions and mass accumulation on a surface were completed. Chemical analyses of liquids and solids were continued to aid in understanding the mechanisms of fuel degradation and solid formation and to guide future testing.

The photon correlation spectroscopy system has been made operational and initial tests have been performed. These tests indicate that particle formation of sizes $<1-10 \mu\text{m}$ dominate early formation and growth at the temperatures tested but that larger particles are eventually formed. Results show that the particle size distribution may be complex, not simply monomodal, but the technique is very sensitive to detecting the initial stages of particle formation. Extensive calibrations were performed at ambient and elevated temperatures. The initial tests have shown that this technique can acquire useful data showing particle size formation and growth as well as provide distributions of diffusion coefficients required for mathematical modeling efforts.

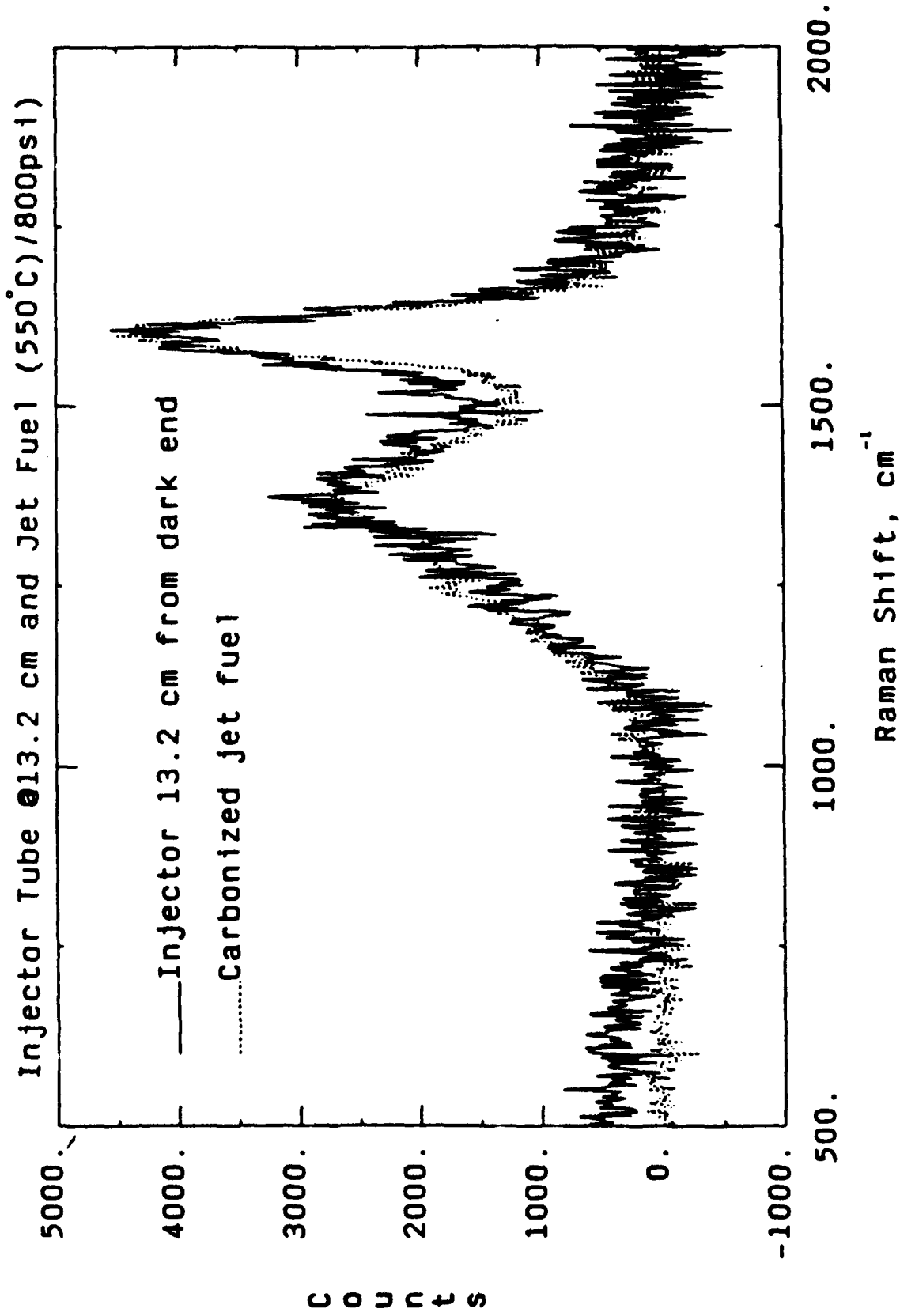


Figure 22. Raman spectra of injector arm (13.2 cm from tube end) compared with carbonization from JP-8 fuel stressed at 550°C.

#6212 013104/3 - Jet Fuel Carbonized at 550°C in Air

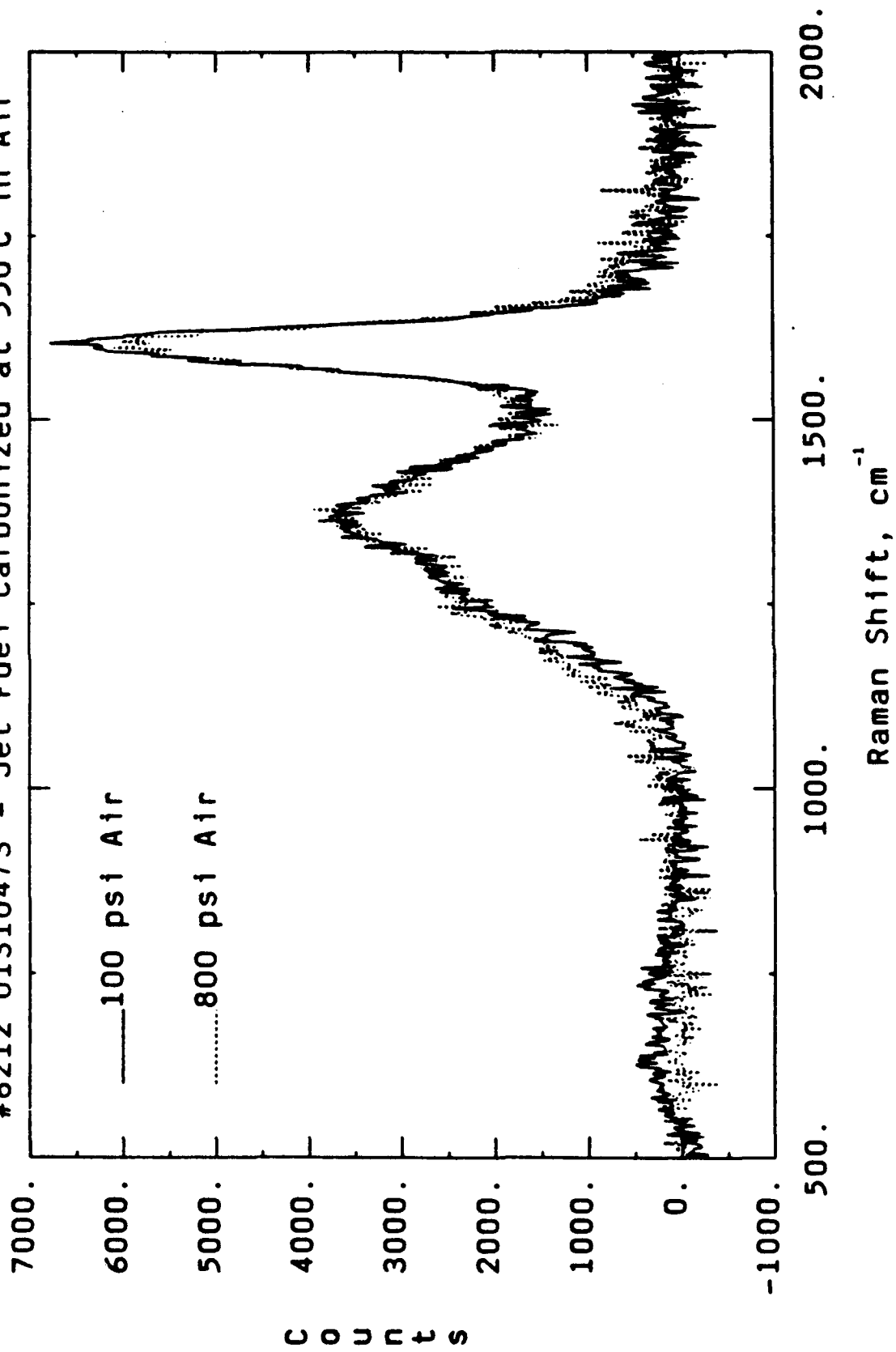


Figure 23. Raman spectra of carbonization from JP-8 fuel stressed at 550°C in air at 100 psi and at 800 psi.

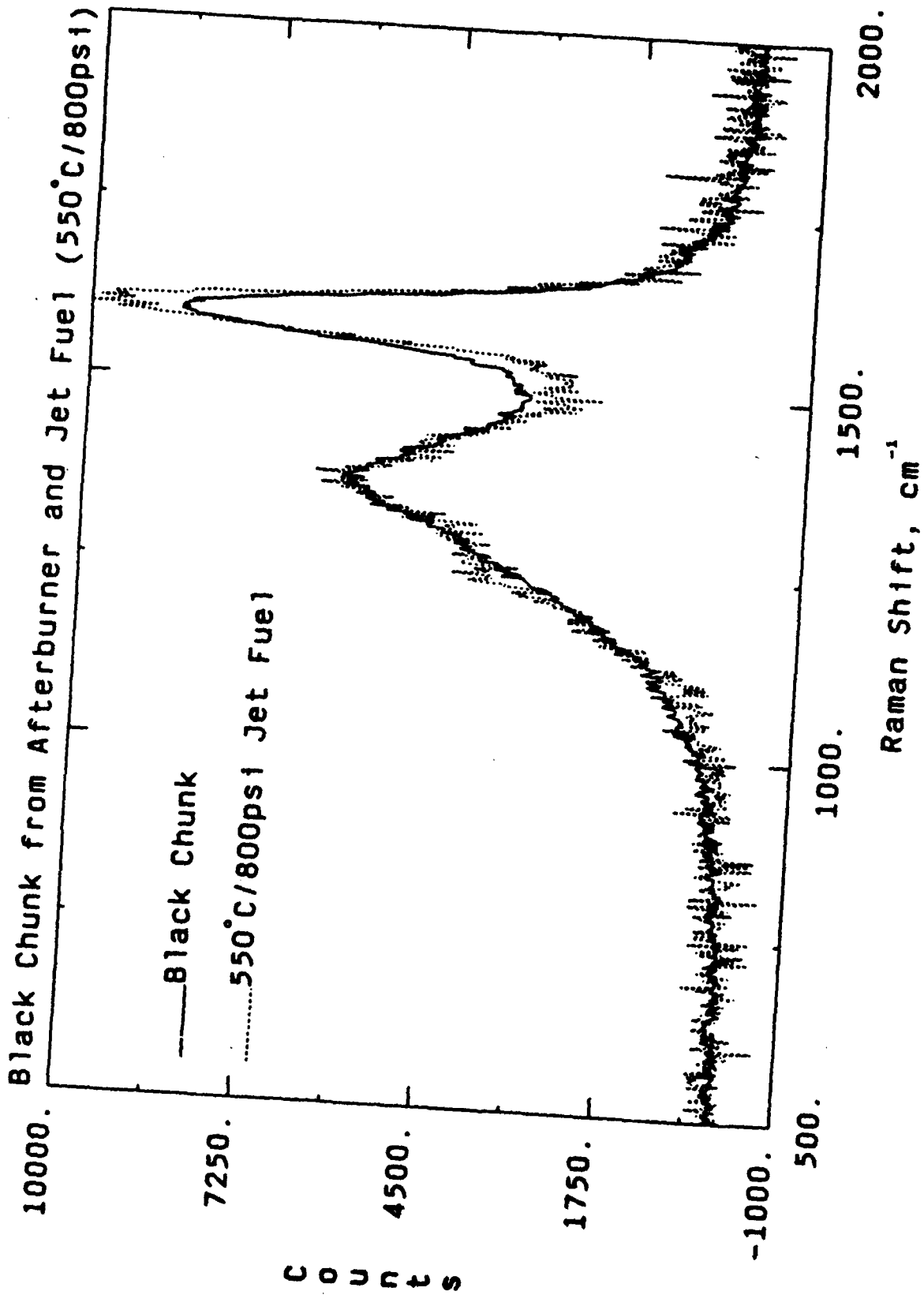


Figure 24. Raman spectra of amorphous deposits from injector arm and carbonization from JP-8 fuel stressed at 550°C.

The acoustic plate mode device, developed to measure mass accumulation on a surface, is extremely sensitive but showed operational difficulties at higher temperatures. A second-generation mass sensor, a quartz crystal microbalance, was developed and has been shown to be more robust. Initial tests have shown that the device can perform at temperatures over 200°C. A system for thermally stressing fuels has been developed around this sensor, along with analysis software. Both mass accumulation values and viscosity values (required for analyzing the photon correlation spectroscopy data) can be extracted from the data.

Batch microautoclave tests were performed to determine solubility effects on solids formed by an oxidative mechanism. The results affirmed the complexity of the chemistry of jet fuel degradation. Visually, degradation of the fuel, as characterized by color and sediment formed, increased as the temperature of the batch isothermal tests was increased to 225°C. However, the extent of fuel degradation apparently decreased at temperatures above 225°C, with the sample tested at 299°C showing little visual evidence of fuel degradation. Additional tests indicated that solids formed at lower temperatures (e.g., 225°C) did not significantly solubilize at higher temperatures, indicating that substantial solid formation may occur in a particular temperature range if the residence time at those temperatures was sufficient. Gas analyses showed that the availability of oxygen is extremely important.

Analyses were performed on an aircraft afterburner injector arm and associated solid deposits. Two distinct types of deposit morphologies were detected and related to the temperature of formation. Raman spectroscopy was used to estimate roughly the temperatures at which the solid were formed. The presence of lower temperature forms of carbon interspersed with higher temperature forms at the location where the majority of the deposits were located suggest that a temperature gradient existed during cool-down and that the thick carbon deposition may be related to carbonization of residual jet fuel.

Fourier transform infrared analyses performed on jet fuel further indicate the importance of the level of oxygen concentration at which tests are performed. When little oxygen is present, FTIR analyses show little change in the stressed liquid; when oxygen is continuously supplied during thermal stressing, substantial changes appear in many of the oxygen-related spectral bands. The tests show that FTIR analyses on liquid fuels should be used primarily when oxygen availability is sufficient.

In summary, instrumentation systems have been developed and testing has been initiated in areas identified as essential to understanding the mechanisms of fuel degradation and deposition. Analyses of jet fuel liquids and solids, as described in this report and in Reference 11, have identified important factors in the decomposition of hydrocarbon fuels at elevated temperatures and will continue to guide test conditions. Studies to be performed during the next year will continue to acquire data necessary to developing global models of particle formation and growth and rate equations describing fuel degradation.

REFERENCES

1. Klavetter, E., O'Hern, T., Marshall, Jr., B., Merrill, R., and G. Frye, "Advanced Thermally Stable Jet Fuels 1990 Annual Report, Volume I", WRDC-TR-90-2079, 1990.
2. Bol'shakov, G. F., The Physico-Chemical Principles of the Formation of Deposits in Jet Fuels, translation from the Foreign Technology Division, USAF, Report No. AD 781164, 1972.
3. Weiner, B. B., "Particle Sizing Using Photon Correlation Spectroscopy," in Modern Methods of Particle Size Analysis, H. G. Barth, Ed. (Wiley, New York, 1984), pp. 93-116.
4. Oliver, C. J., "Correlation Techniques," in Photon Correlation and Light Beating Spectroscopy, H. Z. Cummins and E. R. Pike, Eds. (Plenum, New York, 1974), pp. 151-223.
5. Bott, S. E., "Submicron Particle Sizing by Photon Correlation Spectroscopy: Use of Multiple Angle Detection," Coulter Electronics Technical Report No. T104.
6. Advanced Thermally Stable Jet Fuels Development Program Progress Report for October-December 1990, pp. 1-7.
7. Russo, P., Guo, K., and L. Delong, "A New Look at Distribution Analysis of Dynamic Light Scattering Data, Using Only a Microcomputer," Society of Plastics Engineers, 46th Annual Technical Conference Proceedings, 1988, pp. 983-985.
8. Pecora, R. and B. J. Berne, Dynamic Light Scattering with Applications to Chemistry, Biology and Physics (Wiley, New York, 1976), Chapter 5.
9. Advanced Thermally Stable Jet Fuels Development Program Progress Report for January-March 1991, pp. 1-6.
10. CRC (Coordinating Research Council, Inc.), "Thermal Oxidation Stability of Jet Fuels--A Literature Survey," CRC Report No. 509, Apr. 1979.
11. Schobert, H., "Advanced Thermally Stable Jet Fuels 1991 Annual Report, Volume II", WRDC-TR-91-?, 1991.